Arab J Sci Eng (2017) 42:5121–5145
DOI 10.1007/s13369-017-2618-8

RESEARCH ARTICLE - ELECTRICAL ENGINEERING

Performance Analysis and Experimental Validation of 2-DOF Fractional-Order Controller for Underactuated Rotary Inverted Pendulum

Prakash Dwivedi[1] · **Sandeep Pandey**[2] · **Anjali Junghare**[2]

Received: 7 December 2016 / Accepted: 8 May 2017 / Published online: 29 May 2017

Abstract Several numbers of controllers are developed and implemented to enhance the performance of rotary single inverted pendulum (RSIP). This paper addresses a new two-degree-of-freedom (2-DOF) fractional control strategy for RSIP, which is a composition of feedback and feed-forward paths. Primary controller relates the perturbation attenuation, while the secondary controller is accountable for set point tracking. The pole placement technique is used for the design of 2-DOF proportional integral derivative (2-DOF PID) controller. In order to intensify the potentiality of 2-DOF PID controller, it is supplemented with fractional calculus. The tuning of fractional parameters is done by frequency domain analysis using the Nyquist plot. The proposed 2-DOF fractional-order PID controller is materialized on RSIP system which out turns the outstanding experimental results for both stabilization and trajectory tracking tasks. The system is investigated for stability, sensitivity and robustness, which confirms the ability of the proposed controller to reject the external random perturbations.

Keywords FOPID controller · 2-DOF PID controller · Inverted pendulum · Sensitivity

✉ Prakash Dwivedi
prakashdwivedi@nituk.ac.in

Sandeep Pandey
sanbhu28@gmail.com

Anjali Junghare
asjunghare@eee.vnit.ac.in

[1] Electrical Engineering Department, National Institute of Technology, Uttarakhand, Srinagar 246174, India

[2] Electrical Engineering Department, Visvesvaraya National Institute of Technology, Nagpur 440010, India

1 Introduction

RSIP is fairly a distinct type of tunable mechanical oscillatory system which is intrinsically nonlinear, underactuated, single-input multiple-output system with unstable equilibrium point. These inherent characteristics induce complexity in controlling the system. Therefore, designing a controller for the stabilization of pendulum is a challenging task. This design becomes more complex because of the physical limitations of applied voltage (V), rotational angle (θ_1), pendulum angle (θ_2) and two sensor outputs. A prototype of RSIP shows similitude to the attitude control of a space booster rocket and a satellite, in which rocket assembly should be in a particular position with some angle. The controlling function of RSIP is very similar to an underactuated robotic arm, stabilization of a cabin in a ship, aircraft stabilization in the turbulent air flow, walking of biped animals and robots, etc. Three key aspects have been explored in the literature to control an inverted pendulum. The first aspect explains the swinging up of the pendulum from the original position to functioning position. Second is to stabilize the pendulum link of RSIP system (balancing) at the unstable equilibrium point, and the last aspect is to track control of RSIP (tracing). The main focus in the study is on balancing and tracking of RSIP because of its serviceability in industrial applications.

Numerous control strategies have been proposed in the literature to design a controller for stabilizing RSIP at unstable equilibrium point such as sliding mode control, advanced nonlinear approaches, fuzzy-based compensation, linear feedback stabilization and different conventional-type controllers [1–3]. Each of these methodologies demands complex computations owing to their manifold structure. Conventional PID also known as one-degree-of-freedom PID (1-DOF PID) controller has been universally established for its efficiency to enhance the transients as well as steady-state

performance of RSIP. It has been transpired in the recent years that with the mathematical tools of fractional calculus (FC), numerous phenomena of engineering and other sciences even finance and social sciences can be defined very effectively [4–7]. The necessity of defining a differential operator with an arbitrary order (real, fractional or complex order) is the reason behind the growth of FC. FC provides surplus flexibility for effective treatment of the system in terms of improved performance and stability. The peculiarity of FC in mathematics gives an opportunity to substitute the conventional PID with fractional-order PID (FOPID) in the topology of two-loop PID Controller. Podlubny [8] presented for the first time a FOPID controller with an improved shape of closed-loop response in comparison with PID controller owing to its higher degrees of freedom. Indeed, FOPID is a generalization of traditional PID controller with two supplementary tuning parameters, namely fractional integrator order λ and a fractional differentiator order μ. Because of this advantage, design and performance analysis of a FOPID controller becomes a novel research topic for the researchers. However, the performance of FOPID immensely depends on the tuning procedure. Numerous tuning concepts have been noted in [9–11] to design a FOPID controller. This paper puts forward a tuning technique based on frequency domain specifications, i.e., phase margin (PM) and gain margin (GM).

However, large overshoot has been detected in FOPID controller by virtue of design setback of 1-DOF which holds single feedback loop (set point-to-output transfer function) as it is ineffectual to lockup good tracking and perturbation rejection concurrently. To get rid of these setbacks, another feed-forward loop (disturbance-to-output transfer function) as a pre filter can be blend with feedback FOPID controller for smooth set point tracking. The strategy 2-DOF FOPID controller boosts the disturbance rejection of the closed-loop system while upholding the satisfactory set point response. 2-DOF FOPID controllers for different industrial plants have been investigated by quite a few authors in [12–15]. Here it is a need to mention that 2-DOF FOPID controller is designed and tested on RSIP system for the first time. No related literature is reported earlier.

The paper is authored as follows. Section 2 provides dynamics of RSIP. The design of proposed controllers and tuning method are provided in Sect. 3. Discussion and analysis of experimental results of proposed controllers are covered in Sect. 4. Section 5 presents the concluding remarks.

2 Rotary Inverted Pendulum

The inceptive inverted pendulum model was introduced as a cart type. However, to compensate the limitation of the cart length, RSIP was invented. The benchmark framework of RSIP is shown in Fig. 1a. It is a nonlinear system having two degrees of freedom of motion. Considering the ease of modeling with Lagrangian formulation, it is adopted. The motion of rotating arm is given in (1),

$$\ddot{\theta_1}(J_1+m_2L_1^2) = T_{\text{out}} - m_2l_2L_1(\ddot{\theta}_2\cos\theta_2 - \dot{\theta}_2^2\sin\theta_2) - \beta_1\dot{\theta}_1 \tag{1}$$

The angular position of the pendulum is described as in (2),

$$\ddot{\theta_2}(J_2 + m_2l_2^2) = -m_2l_2g\sin\theta_2 - m_2l_2L_1\ddot{\theta}_1\cos\theta_2 - \beta_2\dot{\theta}_2 \tag{2}$$

Equations (1) and (2) are linearized around small deviation of angle δ as given below.

$$\theta_2 \cong \pi + \delta, \quad \dot{\theta}_2^2 \cong 0, \quad \sin\theta_2 \cong -\delta, \quad \cos\theta_2 \cong -1$$

The reduced equations are given in (3) and (4),

$$\ddot{\theta_1}(J_1 + m_2L_1^2) = T_{\text{out}} + m_2l_2L_1\ddot{\theta}_2 - \beta_1\dot{\theta}_1 \tag{3}$$

$$\ddot{\theta_2}(J_2 + m_2l_2^2) = m_2l_2g\theta_2 + m_2l_2L_1\ddot{\theta}_1 - \beta_2\dot{\theta}_2 \tag{4}$$

Above linearized equations in state space are expressed as in (5) and (6),

$$\begin{bmatrix}\dot{\theta_1}\\ \dot{\theta_2}\\ \ddot{\theta_1}\\ \ddot{\theta_2}\end{bmatrix} = \begin{bmatrix}0 & 0 & 1 & 0\\ 0 & 0 & 0 & 1\\ 0 & \frac{FB}{A} & -\frac{\beta_1}{A} & -\frac{FC}{A}\\ 0 & \frac{B+EFB}{A} & -\frac{E\beta_1}{A} & -\frac{EFC+AC}{A}\end{bmatrix}\begin{bmatrix}\theta_1\\ \theta_2\\ \dot{\theta_1}\\ \dot{\theta_2}\end{bmatrix} + \begin{bmatrix}0\\ 0\\ \frac{1.005}{A}\\ \frac{1.005E}{A}\end{bmatrix}V_m \tag{5}$$

$$y = \begin{bmatrix}1 & 0 & 0 & 0\\ 0 & 1 & 0 & 0\end{bmatrix}\begin{bmatrix}\theta_1\\ \theta_2\\ \dot{\theta_1}\\ \dot{\theta_2}\end{bmatrix} \tag{6}$$

where $A = J_1 + m_2L_1^2 - \frac{m_2^2l_2^2L_1^2}{J_2+m_2l_2^2}$; $B = \frac{m_2l_2g}{J_2+m_2l_2^2}$; $C = \frac{\beta_2}{J_2+m_2l_2^2}$; $E = \frac{m_2l_2L_1}{J_2+m_2l_2^2}$; $F = m_2l_2L_1$ using the physical parameters given in Table 1 [16], the state space is obtained as in (7) and (8),

$$\begin{bmatrix}\dot{\theta_1}\\ \dot{\theta_2}\\ \ddot{\theta_1}\\ \ddot{\theta_2}\end{bmatrix} = \begin{bmatrix}0 & 0 & 1 & 0\\ 0 & 0 & 0 & 1\\ 0 & 52.78 & -0.66 & -0.65\\ 0 & 97.98 & -0.65 & -1.21\end{bmatrix}\begin{bmatrix}\theta_1\\ \theta_2\\ \dot{\theta_1}\\ \dot{\theta_2}\end{bmatrix} + \begin{bmatrix}0\\ 0\\ 274.45\\ 273.92\end{bmatrix}V_m \tag{7}$$

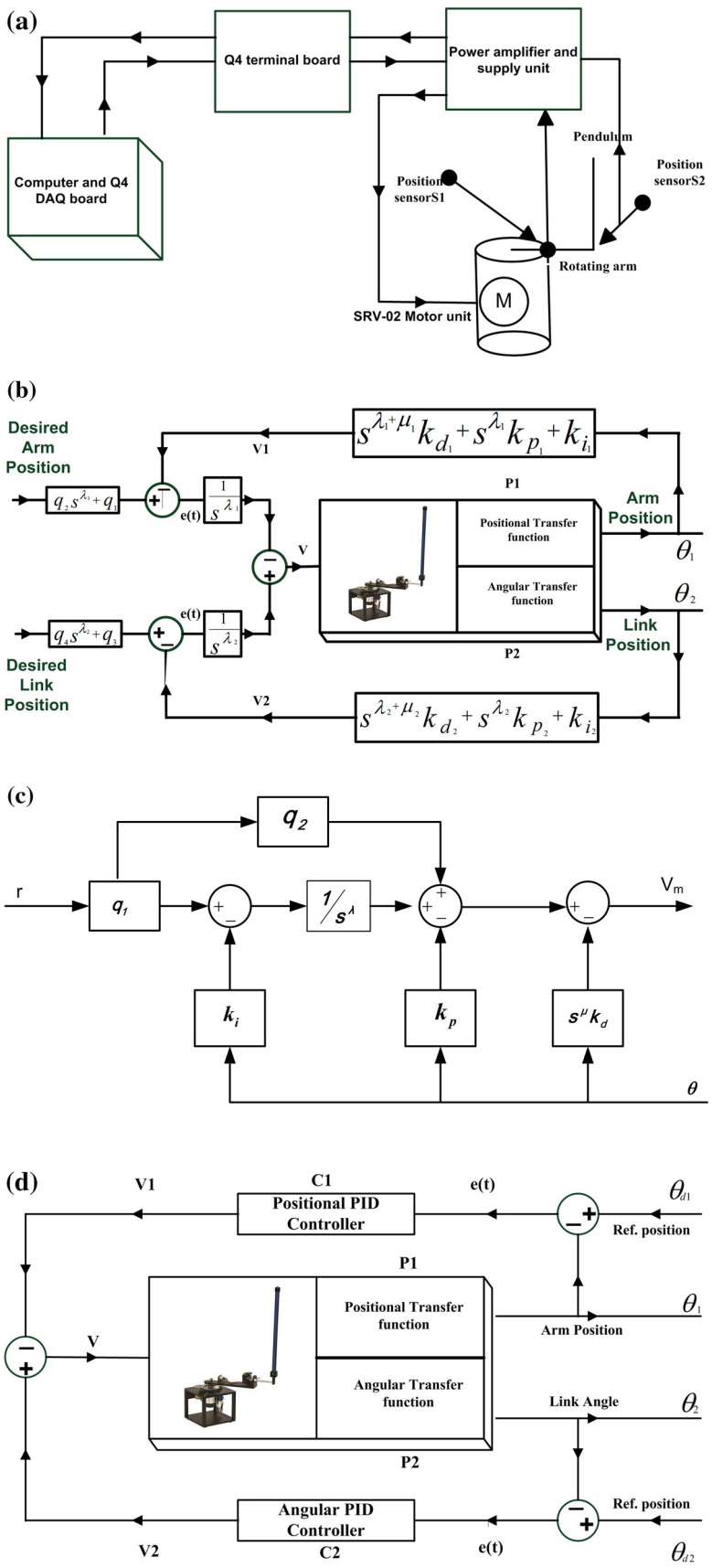

Fig. 1 **a** Investigational setup, **b** 2-DOF control scheme, **c** realization of 2-DOF structure and **d** 1-DOF control structure

Table 1 Physical parameters of inverted pendulum

Parameters description	Notations	Experimental value	Units
Viscous damping coefficient of arm	β_1	0.0024	N-m-s/rad
Viscous damping coefficient of pendulum	β_2	0.0024	N-m-s/rad
SRV-02 system gear ratio	K_g	70	–
Back emf constant	K_m	0.00767	V/(rad/s)
Half-length of pendulum	l_2	0.1675	m
Mass of the pendulum	m_2	0.125	Kg
Rotating arm length	L_1	0.2159	m
Mass of rotary arm	M	0.2570	Kg
Armature resistance	R_m	2.6	Ω
Gearbox efficiency	η_g	0.9	–
Motor efficiency	η_m	0.69	–
Acceleration owing to gravity	g	9.8	m/s^2
Motor torque constant	K_t	0.00767	$N\text{-}m/A$
Moment of inertia of the SRV02 motor	J_{eq}	0.0035842	$kg\text{-}m^2$

$$y = \begin{bmatrix} 1 & 0 & 0 & 0 \\ 0 & 1 & 0 & 0 \end{bmatrix} \begin{bmatrix} \theta_1 \\ \theta_2 \\ \dot{\theta}_1 \\ \dot{\theta}_2 \end{bmatrix} \tag{8}$$

Considering the output variable as rotational arm position θ_1 and pendulum link angle θ_2, the transfer function is obtained as given in (9) and (10),

$$\frac{\theta_1(s)}{V_m(s)} = \frac{274.5s^2 + 154s - 12430}{s^4 + 1.87s^3 - 97.61s^2 - 26.69s} = P_1 \tag{9}$$

$$\frac{\theta_2(s)}{V_m(s)} = \frac{273.9s}{s^3 + 1.87s^2 - 97.61s - 26.69} = P_2 \tag{10}$$

3 Proposed 2-DOF FOPID Controller

3.1 Realization of Fractional-Order Elements

Numerous approximation methods are available in the literature to realize a fractional-order term [17–21]. To implement a fractional-order differentiator and integrator in FOMCON toolbox [22], the Oustaloup's approximation method [18] is used. The slope of the magnitude plot ($\pm\alpha 20$ dB/dec) and phase angle ($\pm\alpha 90°$) for any fractional-order transfer function can be attained by placing an alternate sequence of real poles and zeros on the negative real axis. By fixing a frequency band of interest (ω_b, ω_h) and the error band (ε) around the desired phase angle $\phi_{\text{req}} = \pm\alpha 90°$, a finite order of approximation can be achieved. The Oustaloup's approximation model for a fractional-order differentiator s^α can be written as in (11),

$$\widehat{H}(s) = \left(\frac{\omega_u}{\omega_h}\right)^{\alpha} \prod_{k=-N}^{N} \frac{1 + s/\omega_k'}{1 + s/\omega_k} \tag{11}$$

where

$$\omega_k' = \omega_b \left(\frac{\omega_h}{\omega_b}\right)^{\frac{k+N+1/2-\alpha/2}{2N+1}} \tag{12}$$

and

$$\omega_k^{'} = \omega_b \left(\frac{\omega_h}{\omega_b}\right)^{\frac{k+N+1/2+\alpha/2}{2N+1}} \tag{13}$$

are, respectively, the zeros (12) and poles (13) of rank k and $2N + 1$ is the total number of zeros or poles. Here, ω_b and ω_h are the low and high transitional frequencies and ω_u is the unit gain frequency/transitional frequency.

3.2 Structure and Advantage

Here the author has proposed a novel method of 2-DOF-based controller, because of its competency to improve the quality of set point tracking and disturbance rejection. Block diagram of proposed 2-DOF FOPID controller to be clustered with RSIP system and its realization are shown in Fig. 1b, c, respectively, where C_1 and C_2 are FOPID controllers and written as in (14) and (15),

$$C_1(s) = K_{p1} + s^{\mu 1} K_{d1} + \frac{K_{i1}}{s^{\lambda 1}} \tag{14}$$

$$C_2(s) = K_{p2} + s^{\mu 2} K_{d2} + \frac{K_{i2}}{s^{\lambda 2}} \tag{15}$$

The characteristic equation for the control structure presented in Fig. 1b is expressed as in (16),

$$1 - P_1C_1 + P_2C_2 = 0 \tag{16}$$

1-DOF FOPID control scheme for the same system is shown in Fig. 1d. The characteristic equation of both the control scheme is found to be same as in (16). Therefore, the loop robustness of both the schemes for a set of the tuned parameters $k_{p1}, k_{i1}, k_{d1}, k_{p2}, k_{i2}, k_{d2}, \lambda_1, \lambda_2, \mu_1$ and μ_2 are same. The response of 1-DOF FOPID shows large overshoot due to two additional zeros introduced in the closed-loop transfer function because of PID terms. In 2-DOF FOPID controller, locating the PID controller in the feedback path removes the zeros from closed-loop transfer function. To augment this, four more parameters for gain q_1, q_2, q_3 and q_4 (gain of the feed-forward loop) assist in adding a zero at desired position to achieve the refined performance.

3.3 Design

The first step in the design of 2-DOF PID is to initialize all the feed-forward parameters to zero. Next, the gain parameters of two-loop FOPID controllers are determined using pole placement technique deploying LQR method. Considering the angle of a pendulum with extreme vitality, given weightage of θ_2 is 100. Therefore, an appropriate combination was taken of $Q = \text{diag}[1, 100, 0, 0]$ and $R = 10$ for finding the gain matrix K. The obtained parameters of state feedback matrix K are as below:

$$K_1 = -0.31623, \quad K_2 = 4.5308, \quad K_3 = -0.24353,$$
$$K_4 = 0.40985$$

Therefore, closed-loop poles of the modified system are as follows:

$$s = -22.0779 \pm j19.7108, -1.5705 \pm j1.422$$

To retain the robustness behavior of LQR in two-loop PID design, use above four poles with choosing the fifth pole at $s = -\alpha$ (six times away from the real part of dominant pole to confirm the loop robustness and better disturbance rejection), the characteristic equation of integer-order PID (IOPID)-compensated closed-loop system can be represented as (17),

$$s^5 + 56.7s^4 + 1465s^3 + 12550s^2 + 31720s + 37050 = 0 \tag{17}$$

Substituting the terms P_1, P_2, C_1, C_2 as defined earlier in (9), (10), (14), (15) and $\lambda_1 = \lambda_2 = \mu_1 = \mu_2 = 1$ in (16), the expression reduces to characteristic equation of IOPID-compensated closed-loop system presented in (18),

$$\begin{aligned} &s^5 + s^4(1.87 - 274.5k_{d1} + 273.9k_{d2}) \\ &+ s^3(-97.61 - 154.1k_{d1} - 274.5k_{p1} \\ &+ 273.9k_{p2}) + s^2(-29.69 + 12430k_{d1} \\ &- 154.1k_{p1} - 274.5k_{i1} + 273.9k_{i2}) \\ &+ s(12430k_{p1} - 154.1k_{i1}) + 12430k_{i1} = 0 \end{aligned} \tag{18}$$

Here for two-loop PID controller, the dominance of the poles is retained as in LQR method, and two Eqs. (17) and (18) can be compared. After comparing, five equations are obtained with six unknowns. On choosing k_{d2}=1, the following PID parameters are obtained

$$k_{p1} = 2.588, \quad k_{i1} = 2.9806, \quad k_{d1} = 0.798$$
$$k_{p2} = 8.7476, \quad k_{i2} = 14.15722, \quad k_{d2} = 1.0$$

To reduce the complexity for tuning the fractional parameters $\lambda_1, \lambda_2, \mu_1$ and μ_2, frequency domain technique is used. Here, the author proposes a tuning algorithm to tune the four unknown parameters $\lambda_1, \lambda_2, \mu_1$ and μ_2. Assumptions made in tuning algorithm are as follows:

- In order to reduce the complexity in tuning procedure of fractional-order operators, it is assumed that fractional operators λ_1 and λ_2 are equal to λ.
- Operator λ does not affect the PM, and it reduces the steady-state error.
- $\pm 3\%$ variation in GM of PID-compensated plant is acceptable.

Algorithm for tuning the unknown parameters is given in flowchart shown in Fig. 2. The uncompensated open-loop RSIP has four poles with one pole in right side of s-plane. According to Nyquist stability criterion, the Nyquist plot must encircle the critical point $(-1 + j0)$ of the $q(s)$ plane once in the counterclockwise direction for the system to be stable. Figure 3 shows the Nyquist plot of PID-compensated plant with encirclement in anticlockwise direction. It is clearly noted that system is stable with PM and GM being 63.3° and −13.7 dB, respectively.

As given in step 2 of flowchart, vary the value of $\mu_1 \in (0, 2)$ and plot against PM as shown in Fig. 4a. It is noted from Fig. 4a that the maximum PM = 95.3° is achieved at $\mu_1 = 0.86$. As per step 4 using the value of $\mu_1 = 0.86$ and $\lambda = 1$, vary $\mu_2 \in (0, 2)$ and plot the variation in PM as shown in Fig. 4b. Using the empirical relation $\frac{\text{PM}}{100} = \zeta$, PM ≥ 100°, gives $\zeta \geq 1$ which leads the system to be overdamped and sluggish. Therefore, from Fig. 4b it is noted that for $\mu_2 > 1$, PM becomes more than 100°, which will make

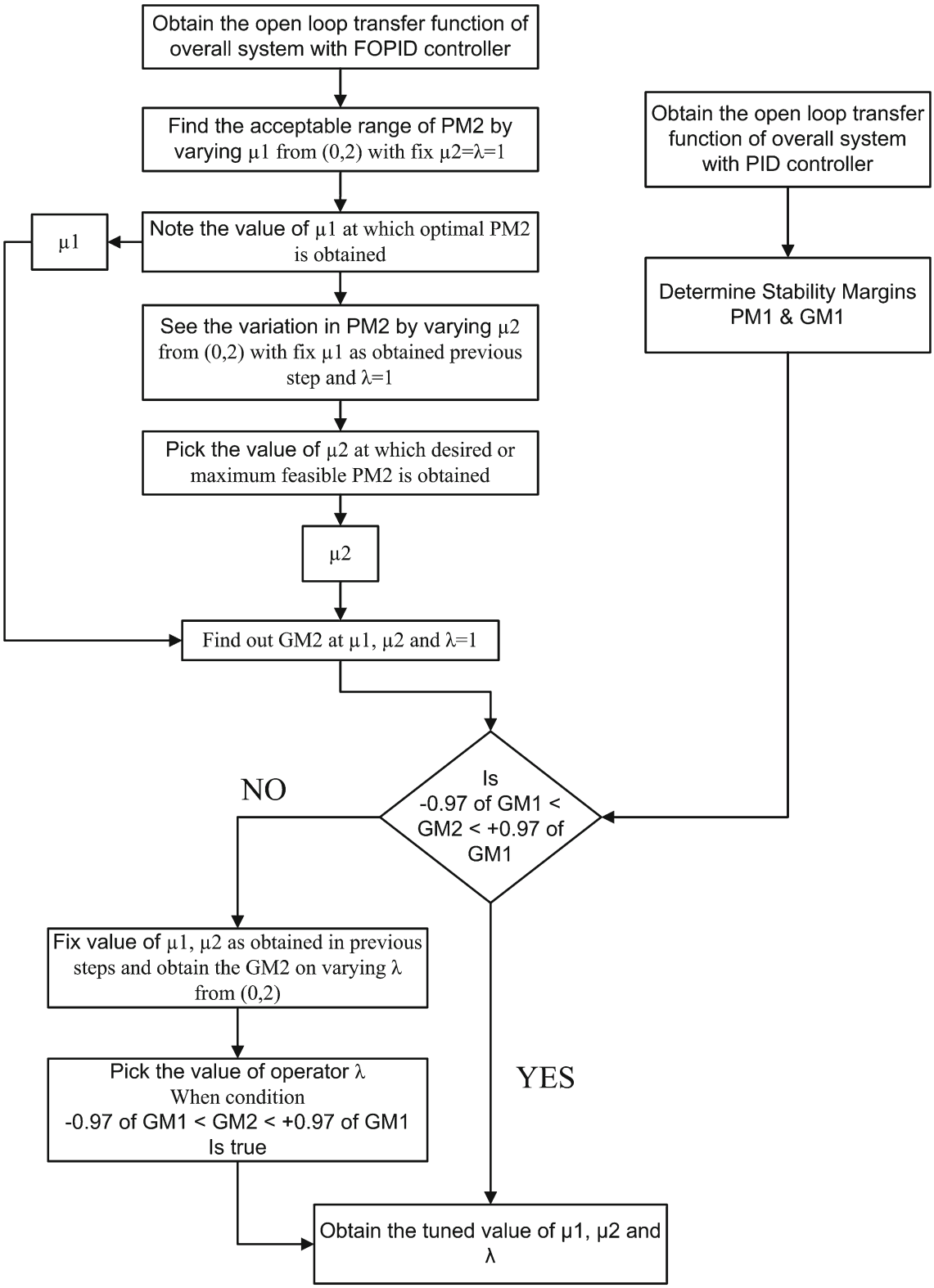

Fig. 2 Flowchart of tuning algorithm for fractional controller

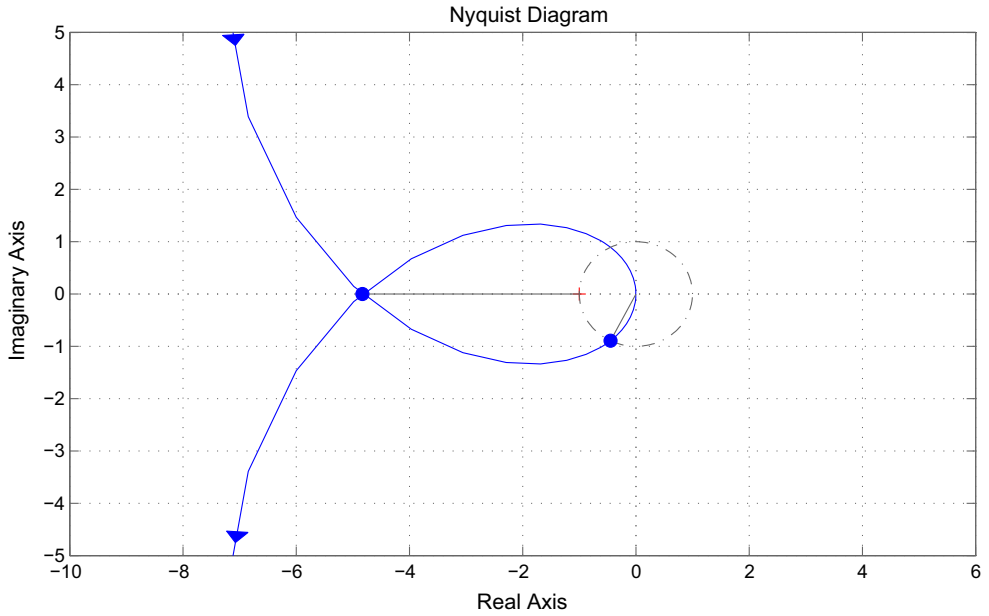

Fig. 3 Nyquist plot of PID-compensated plant

system sluggish. In order to make the system faster, μ_2 is chosen as 1 whose corresponding PM is 95.3°. In this case, GM $= -11.9$ dB which is less than 3% of PID-compensated GM as observed from Fig. 4c.

To compensate the decrease in GM, the value of λ is varied between 0 and 2 as shown in Fig. 4d (step 9). It is observed that at $\lambda = 0.75$, ± 14.1 dB, GM is achieved which is within the desired tolerance. Variation in fractional parameters and corresponding changes in stability margins and sensitivity peak are presented in Table 2. Therefore, from step 11 the tuned values of FOPID controller are obtained as follows:

$$\lambda = 0.75 = \lambda_1 = \lambda_2, \mu_1 = 0.86 \text{ and } \mu_2 = 1$$

Nyquist plot of FOPID-compensated system with these tuned values is shown in Fig. 5. From Fig. 5, it is noted that GM of PID-compensated system and FOPID-compensated system is nearly equal to each other. However, there is an increment of 32° in PM of the overall system with FOPID controller. It makes the system more robust. This is verified with the experimental results, phase trajectories and stability analysis, discussed further in Sect. 4.

However, for robust steady-state tracking feed-forward parameters of 2-DOF FOPID need to be tuned accurately. When $\frac{\theta_1}{r} = \frac{\theta_2}{r} = 1$ at, $s = 0$, the feed-forward gains q_1 and q_3 are obtained as

$$q_1 = 2.9806 \text{ and } q_3 = 0$$

Further to obtain the desired speed of response, q_2 and q_4 are required to be tuned. The system performed satisfactory for $q_2 = 2.65$ and $q_4 = 0.5$ after many trials. Here it should be noticed that in proposed topology, 14 parameters have to be tuned for a robust system. Therefore, using pole placement technique, integer-order parameters have been computed. A sophisticated graphical method based on Nyquist criterion has been used to tune the fractional-order parameters. The variables described in feed-forward path have been obtained for precisely tracking the input. Thus, the derivations and computations mentioned in this section clearly show the complexity of the obtained parameters.

4 Results and Discussion

In this section, an experimental analysis and performance assessment of the proposed 2-DOF fractional controller are put forward using RSIP system. Several types of PID controllers have been successfully implemented for RSIP prior to this. Here author claims that this is the first attempt for an experimental demonstration using a novel concept of 2-DOF FOPID with successful implementation for RSIP system. This section is divided into five subsections. At first, experimental framework and software tools are explained. The second subsection addresses the experimental demonstration of 1-DOF FOPID. In the third subsection, 2-DOF PID is discussed with the experimental response, and in fourth subsection, observations of 2-DOF FOPID are given. At the end, robustness and stability have been discussed. In order to visualize the superiority of 2-DOF FOPID controller over 1-DOF FOPID and 2-DOF PID controller, their comparison is presented. In all the cases, pendulum swung up manually

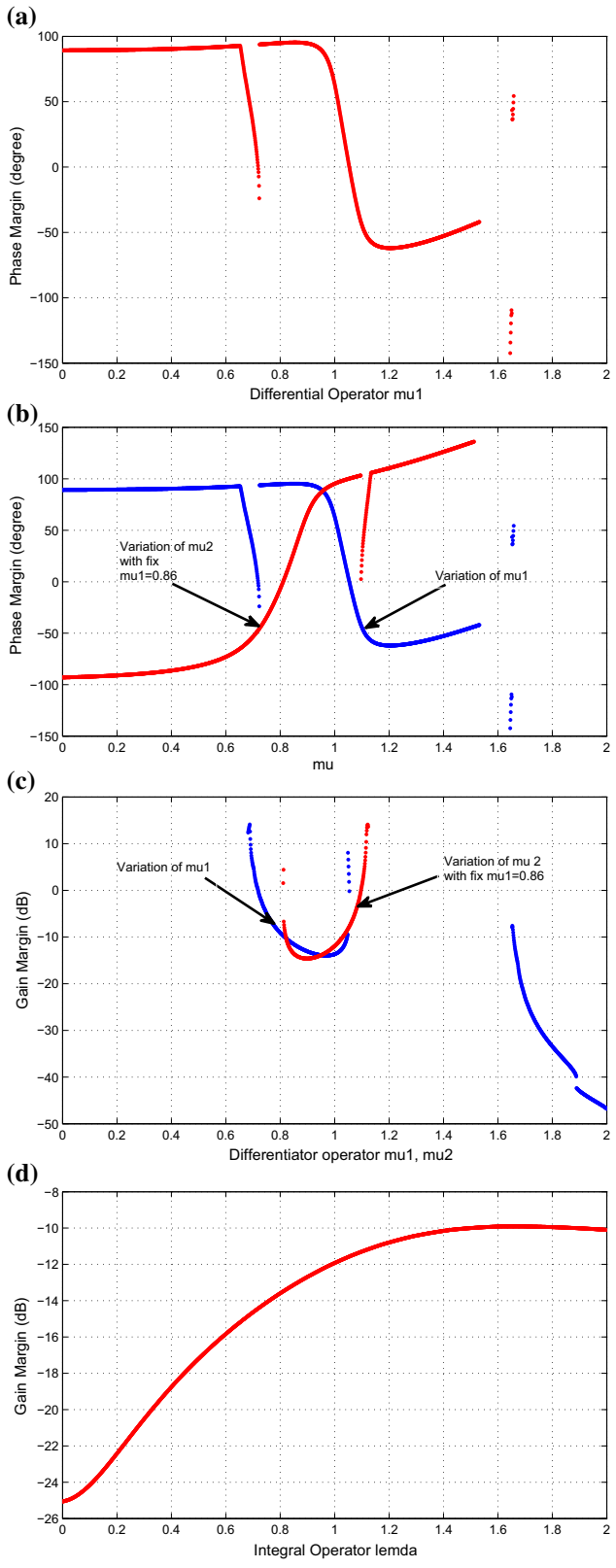

Fig. 4 Variation in **a** PM versus $\mu 1$, **b** PM versus $\mu 1$ and $\mu 2$, **c** GM versus $\mu 1$ and $\mu 2$ and **d** GM versus λ

Table 2 Variation in fractional parameters and corresponding changes in stability margins

Controller	μ_1	μ_2	λ	PM	GM	M_p (dB)
PID	1	1	1	63.3	$\pm$13.7	1
FOPID	0.9	1	1	94.6	$\pm$13.1	−0.00095
	0.86	1	1	95.3	$\pm$11.9	−0.00085
	0.8	1	1	94.9	$\pm$9.12	−0.00061
	0.86	0.9	1	66.2	$\pm$14.6	−0.0713
	0.86	1	0.8	95.2	$\pm$13.3	−0.00085
	0.86	1	0.75	95.2	$\pm$14.1	−0.00085
	0.86	1	0.7	95.2	$\pm$14.6	−0.00085

to bring it to stabilization region. Therefore, the response of the same starts from −3.14 rad or −180°.

4.1 Experimental Framework

The experimental setup of RSIP consists of a mechanical unit (Quanser model SRV-02 ROTPEN) as shown in Fig. 6a. This unit is equipped with a Faulhaber coreless DC motor model 2338S006, two optical encoders, one potentiometer and one tachometer. The control interface between the mechanical unit and computer has been made using an analog control interface (Quanser Q4 DAQ board). The position of the rotational arm and pendulum link sensed by the optical encoder is converted to a digital signal using the Q4 DAQ board, which is connected to the Q4 terminal board through SCSI cable. The terminal board provides connectors for the input and output of the Q4 DAQ board in the computer. Since the analog out ports of the terminal board are not efficient enough to drive the DC motor, it is mandatory to amplify the signal. A 5-pin-DIN to RCA connector is used to connect the DAQ terminal board from power module Quanser 1503 for proper power amplification. However, the gain of a power amplifier is unity, but the amplifier provides much higher current than the DAQ board. To implement the control law in the computer, MATLAB is used as the application host environment. It includes MATLAB/Simulink, FOMCON toolbox [22], real-time workshop (RTW) and QuaRC Simulink development environment. Here Simulink provides the well-structured GUI to realize the control algorithm. RTW generates and executes C++ code from Simulink diagram, state flow charts and MATLAB functions. Quansers rapid prototyping and production system for real-time control (QuaRC) integrates seamlessly with Simulink to allow Simulink models to run in real time in windows as shown in Fig. 6b.

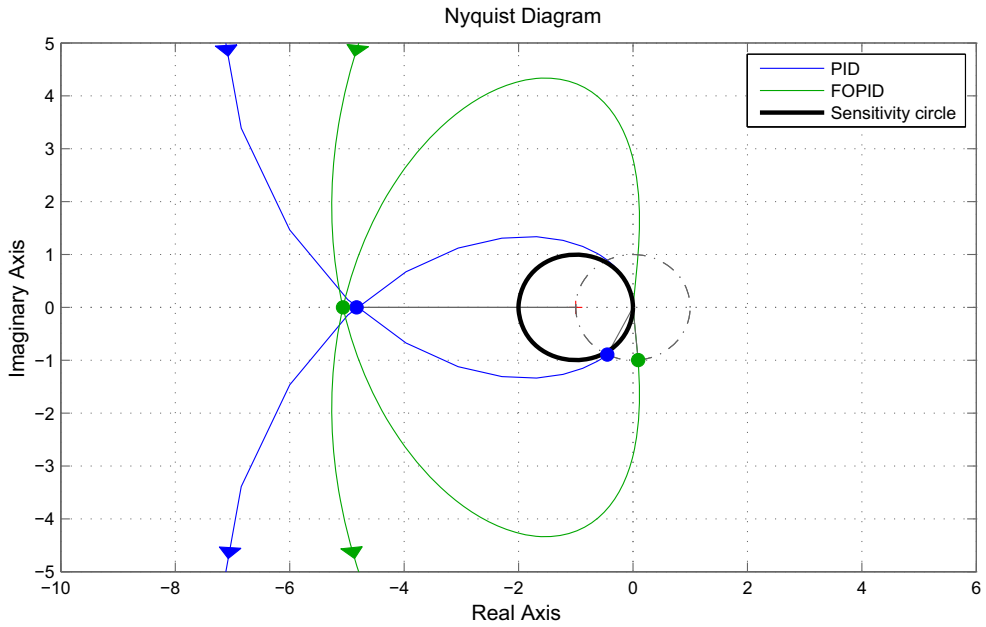

Fig. 5 Nyquist plot of PID- and FOPID-compensated plant with sensitivity circle

4.2 Experimental Results of 1-DOF FOPID

In this section, authors proceed to demonstrate the experimental outcomes of the real RSIP system, when 1-DOF FOPID controller is employed. Figure 1d shows the closed-loop control scheme used in this trial. The sampling time is 0.001 s. Figure 7a renders the trajectory tracking of the rotational arm position. It is noticed that rotational arm follows the desired path with sustained oscillations. Figure 7b shows the experimental results of pendulum angle. It is observed that the pendulum link shows the stable behavior with tracking of the required path. Figure 7c shows the required control signal. The IAE values for the angular deviation of the rotational arm and pendulum link are 0.0443 and 0.07, respectively. The ISE values for the same are 0.0293 and 0.0143, respectively. The peak value of sensitivity function and sensitivity of the system are −0.00085 and 0.97 dB, respectively.

Figure 8a describes a two-dimensional phase portrait which contains the information of rotational position arm and derivative of it. It is found that without loss of controllability, the pendulum is driven to the equilibrium point through a disturbance track and remains at zero position with oscillations. The distance between the points of phase trajectory and equilibrium point specifies the amount of energy in the system at that moment. Here, manually the pendulum link is lifted from −180° to 0° and is seen from Fig. 8b. Later due to controller action, the trajectory converges on the equilibrium point.

Further, the same controller is tested with sawtooth input to check the effect at the time of sudden change in reference trajectory as shown in Fig. 9. All the three variables θ_1, θ_2 and control voltage V show consistent oscillations and large overshoot at the time of sudden change in reference track. It is also observed that the control voltage (V) reached the saturation limit at every sudden change in input. The observed IAE values for the angular deviation of both the links are 1.8 and 2.174 and ISE values are 0.1345 and 0.1589.

4.3 Experimental Results of 2-DOF PID

In this subsection, 2-DOF PID controller is employed to mitigate the oscillations. In Fig. 10a, an astonishing reduction is observed in the oscillations during steady state with reference to 1-DOF FOPID controller. Nonetheless, it is also noted that the difference still persists between the desired set point and experimental position. The observed IAE and ISE values for the angular deviation of the rotational arm are 0.0181 and 0.0093, respectively. Pendulum link position and control voltage show minor changes from the one observed in 1-DOF FOPID controller as shown in Fig. 10b, c. The IAE and ISE values noted for the angular deviation in pendulum links are 0.047 and 0.01807, respectively. Figure 11a, b illustrates the phase trajectories of the rotational arm and pendulum link, respectively.

The response of the sawtooth input as seen in Fig. 12 confirms the potentiality of feed-forward loop in 2-DOF PID controller. Here, the amplitude of the sustained oscillations in the steady state has been reduced as seen in Fig. 12a. The spikes observed during sudden change in the angular position of rotational arm, pendulum link and control voltage in 1-

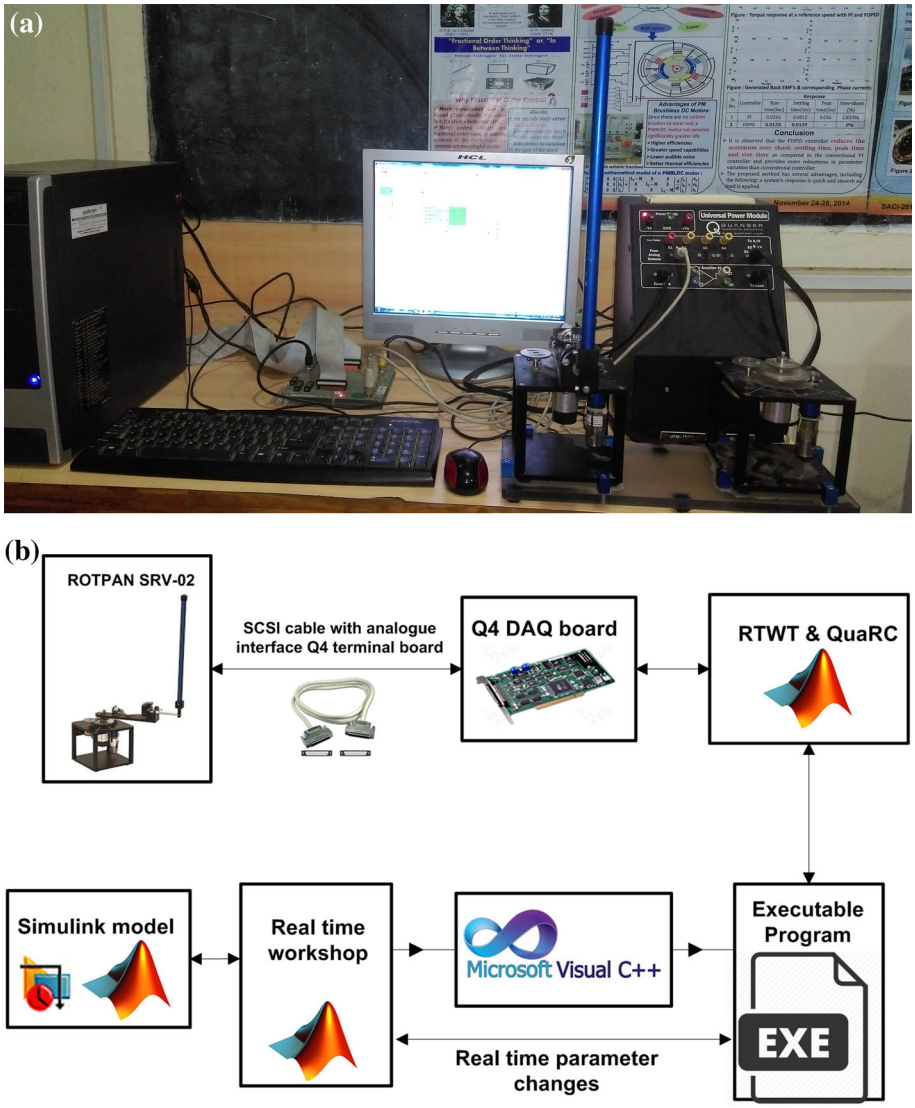

Fig. 6 **a** Experimental framework and **b** control scheme development flow diagram

DOF FOPID got subsided in the response with 2-DOF PID as seen in Fig. 12a–c. The IAE values of 2-DOF PID controller for the angular deviation in rotational arm and pendulum link are 0.2807 and 0.3112, respectively. The ISE values for the same are 0.1176 and 0.031, respectively.

4.4 Experimental Results of 2-DOF FOPID

To ameliorate the regulation of RSIP system, a novel 2-DOF FOPID controller is proposed as shown in Fig. 1b. Figure 13 shows the experimental outcomes of RSIP system when 2-DOF FOPID controller is employed. Figure 13a shows that arm position θ_1 has remarkably reduced oscillations, as compared to 1-DOF FOPID controller and deviations have been diminished between the desired set point and experimental position as compared to 2-DOF PID. This response validates the statement mentioned in Sect. 3.2 that "the improvement in the quality of set point tracking, as well as the disturbance rejection, is a unique feature of the 2-DOF controller." The initial overshoot occurring due to sensor offset is seen in all the cases. Pendulum link position and control voltage show minor change while employing 2-DOF FOPID as shown in Fig. 13b, c. To avoid actuator saturation, here back-calculation anti-windup technique is used. The IAE values for the angular deviation of rotational arm and pendulum link are 0.0087 and 0.0152, respectively. The ISE values for the same are 0.0017 and 0.0074, respectively.

Figure 14a, b illustrates the phase trajectories of rotational arm and pendulum link, respectively. Note that the reduced amplitude of the oscillations is the outcome of the applied control strategy. The lesser distance between the points of phase trajectory and equilibrium point as compared to 1-DOF FOPID and 2-DOF PID indicates that the less amount of energy is required at that moment.

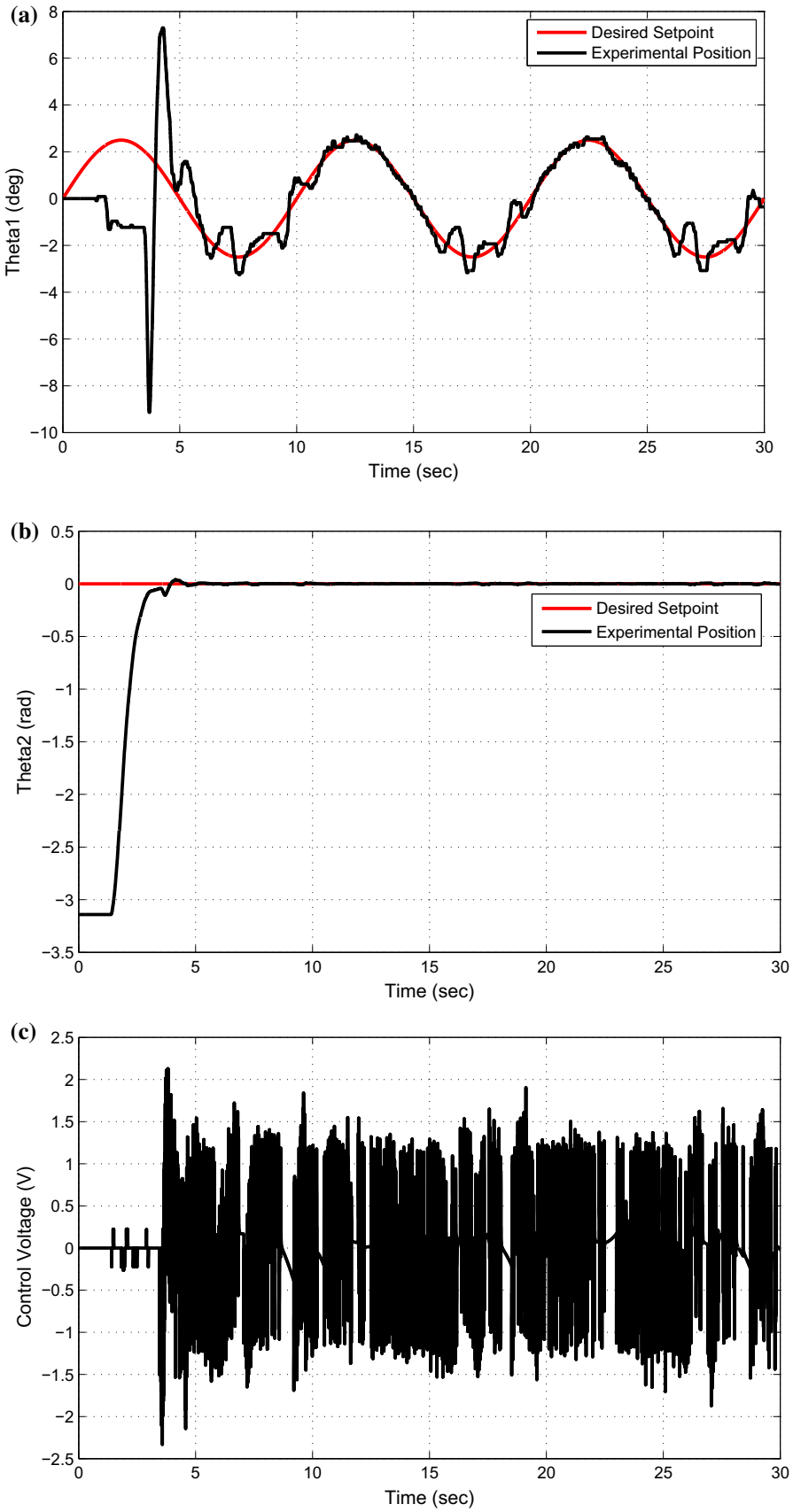

Fig. 7 Experimental results of 1-DOF FOPID controller with sine wave as reference trajectory **a** rotational position $\theta 1$, **b** pendulum link position $\theta 2$ and **c** control voltage

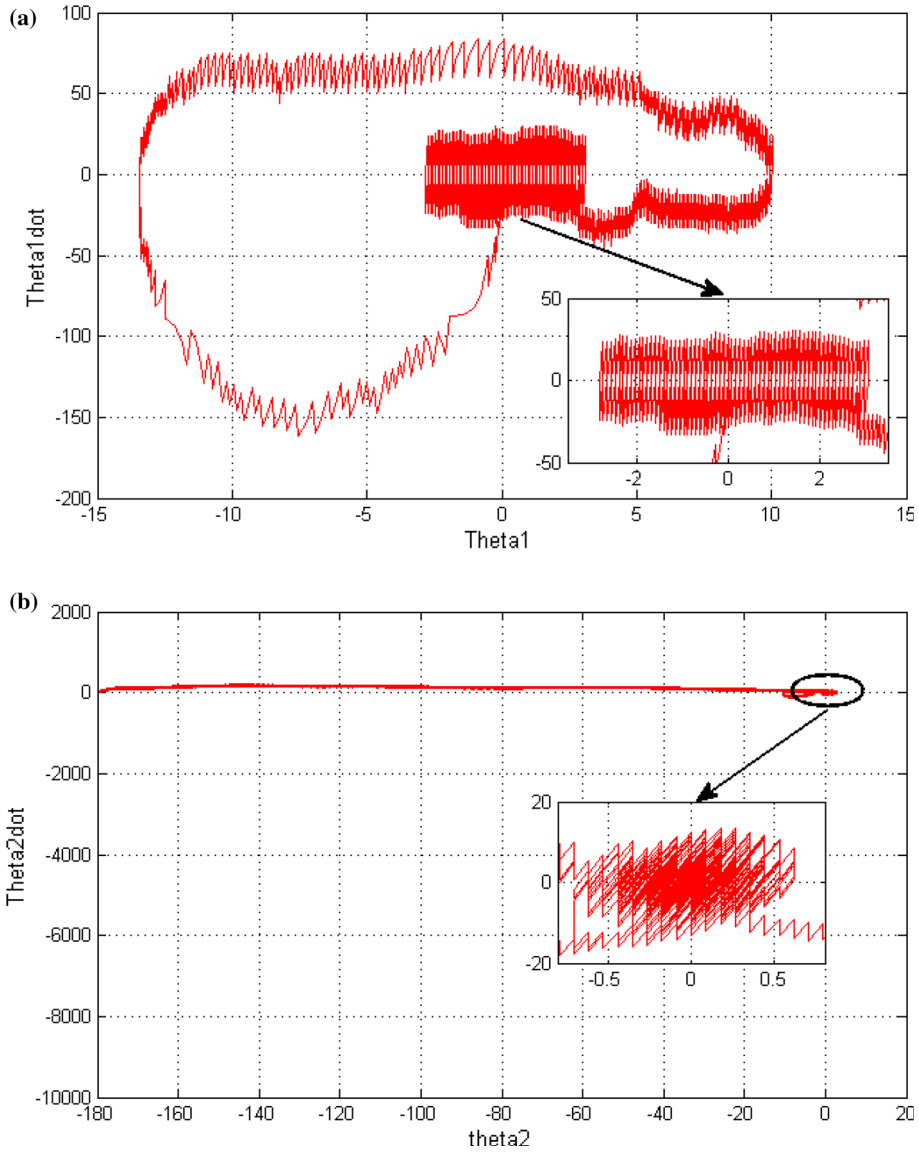

Fig. 8 Phase portrait of 1-DOF FOPID **a** rotational arm and **b** pendulum link

As mentioned in Sect. 3.2, the 2-DOF control scheme reduces the large overshoot owing to absence of zeros in closed-loop transfer function. To authenticate this ability of feed-forward block in 2-DOF FOPID controller, a sawtooth reference input is applied to system as shown in Fig. 15. Here it is noteworthy that sustained oscillations mostly died out as seen from Fig. 15a. Further spikes have been reduced in case of rapid change in the reference trajectory, which is shown in Fig. 15a, b. The same changes are also observed in Fig. 15c, which shows the response of required control voltage. The observed IAE values of 2-DOF FOPID controller for the angular deviation in the rotational arm and pendulum link are 0.1707 and 0.1903, respectively. The ISE values for the same are 0.00489 and 0.01, respectively. Referring to Table 3, it is observed that there is a significant improvement in the response of rotational arm and pendulum link. Figures 9c, 12c and 15c show that the average voltage consumed by plant (when 2-DOF FOPID employed) is comparatively less. The observed performance indices IAE and ISE for angular deviation in rotational arm and pendulum link are given in Table 4. In Table 4, it is inferred that the variations in IAE and ISE values of rotational arm (link 1) and pendulum link (link 2) for 2-DOF FOPID controllers remain smaller as compared to 2-DOF PID as well as FOPID controllers. Table 5 presents the changes in performance indices (IAE and ISE) with variation in feed-forward parameters q_1, q_2, q_3 and q_4. When q_1, q_2, q_3 and q_4 values are either increased or decreased, the performance indices (IAE and ISE) values increased; this implies the efficient choice of the tuned parameters.

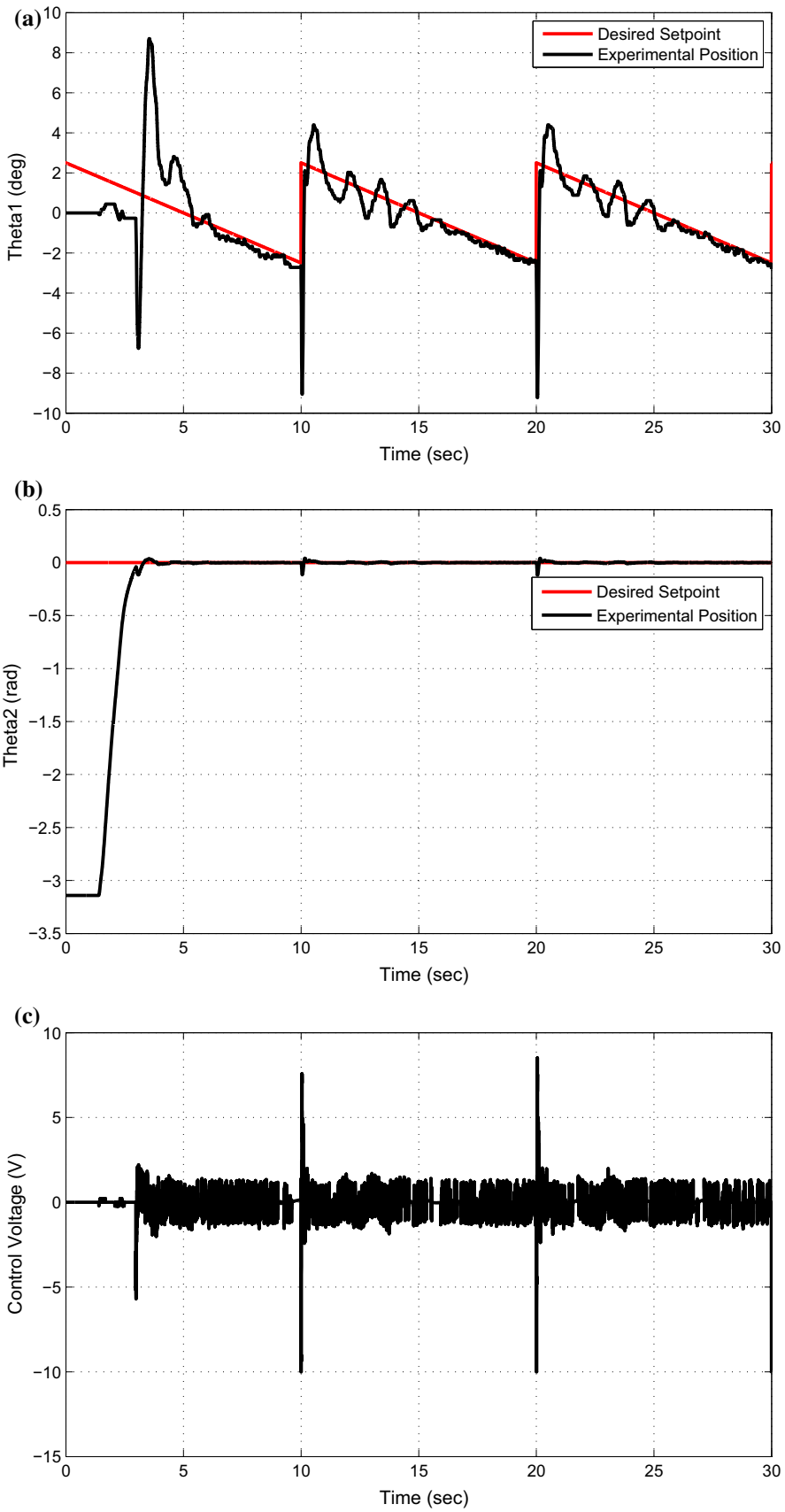

Fig. 9 Experimental results of 1-DOF FOPID controller with sawtooth wave as reference trajectory **a** rotational position $\theta 1$, **b** pendulum link position $\theta 2$ and **c** control voltage

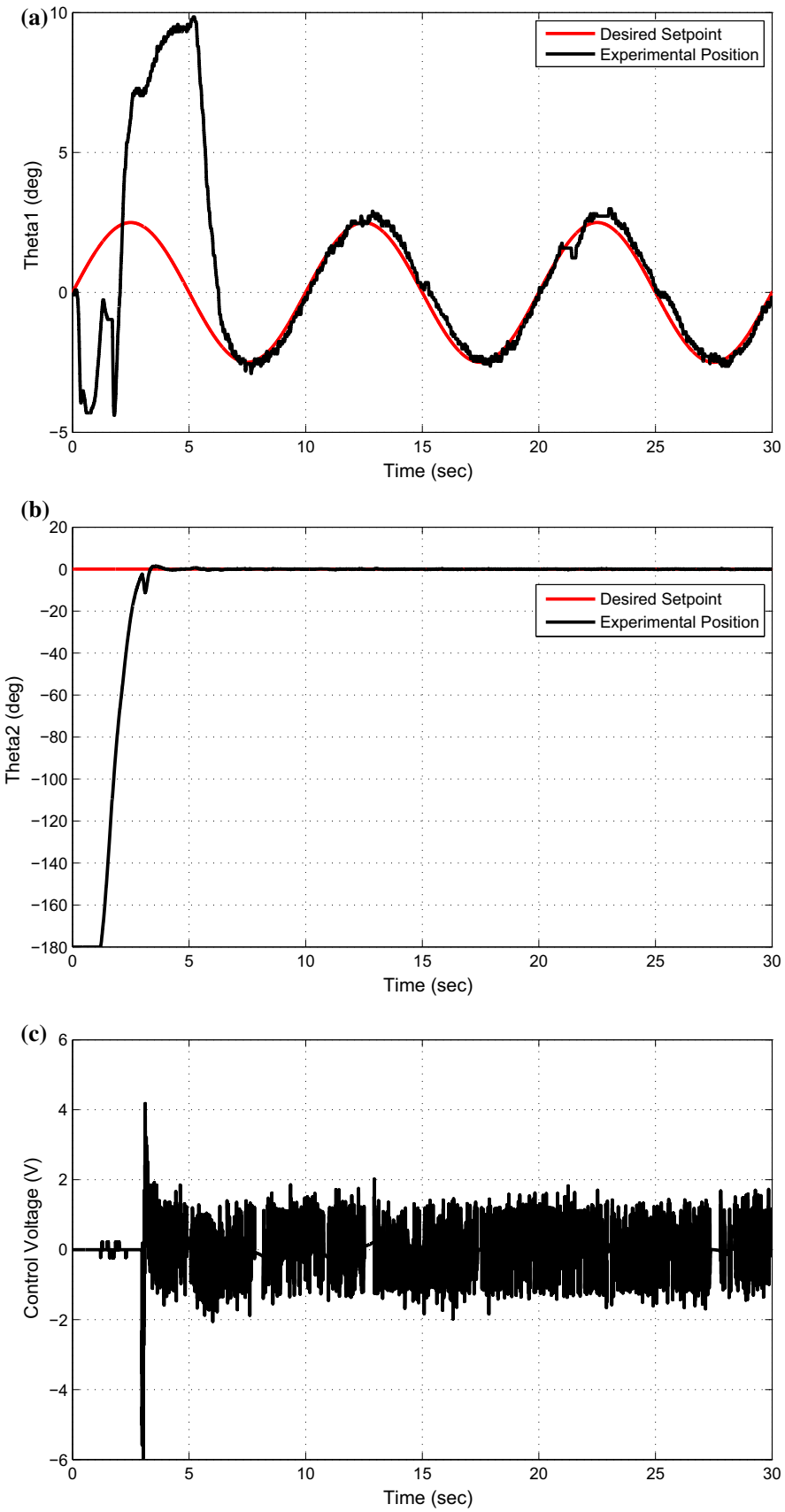

Fig. 10 Experimental results of 2-DOF PID controller with sin wave as reference trajectory **a** rotational position $\theta 1$, **b** pendulum link position $\theta 2$ and **c** control voltage

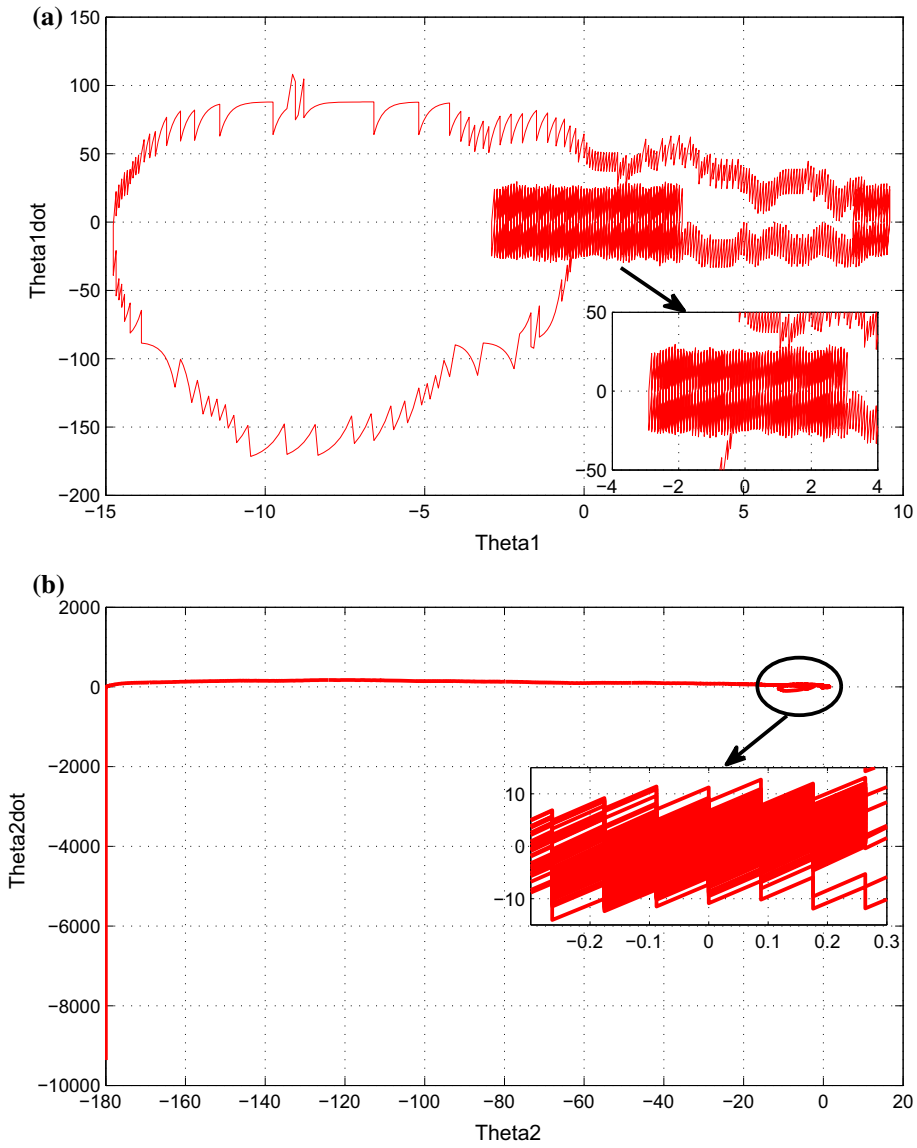

Fig. 11 Phase portrait of 2-DOF PID **a** rotational arm and **b** pendulum link

4.5 Robustness and Stability

4.5.1 Robustness

The robustness is measured using the sensitivity function and its complimentary sensitivity function. Sensitivity function expresses the amount of rejection to the disturbance, and complimentary function is related to the set point tracking performance. The mathematical representations of these functions are given in (19),

$$S_\infty = \frac{1}{1+L} \text{ and } T_\infty = \frac{L}{1+L} \tag{19}$$

where L is the loop transfer function, which is expressed as in (20),

$$L = P_2C_2 - P_1C_1 \tag{20}$$

Peak value of sensitivity function M_p is used further for determining the robustness and describes in (21),

$$M_\mathrm{p} = \sup_\omega |S(j\omega)| \tag{21}$$

Practically to ensure acceptable robust design, the sensitivity value attained is expected to be less than 2. This restriction when referred to the frequency response means GM and PM should be $\geq$2 dB and $\geq$30°, respectively [23]. The robustness is determined in Fig. 5 by sketching the Nyquist plot and adding the circle using the information of sensitivity function. The minimum distance from critical point $(-1 + j0)$ to Nyquist plot is denoted as $d_\mathrm{min} = \frac{1}{M_\mathrm{p}}$

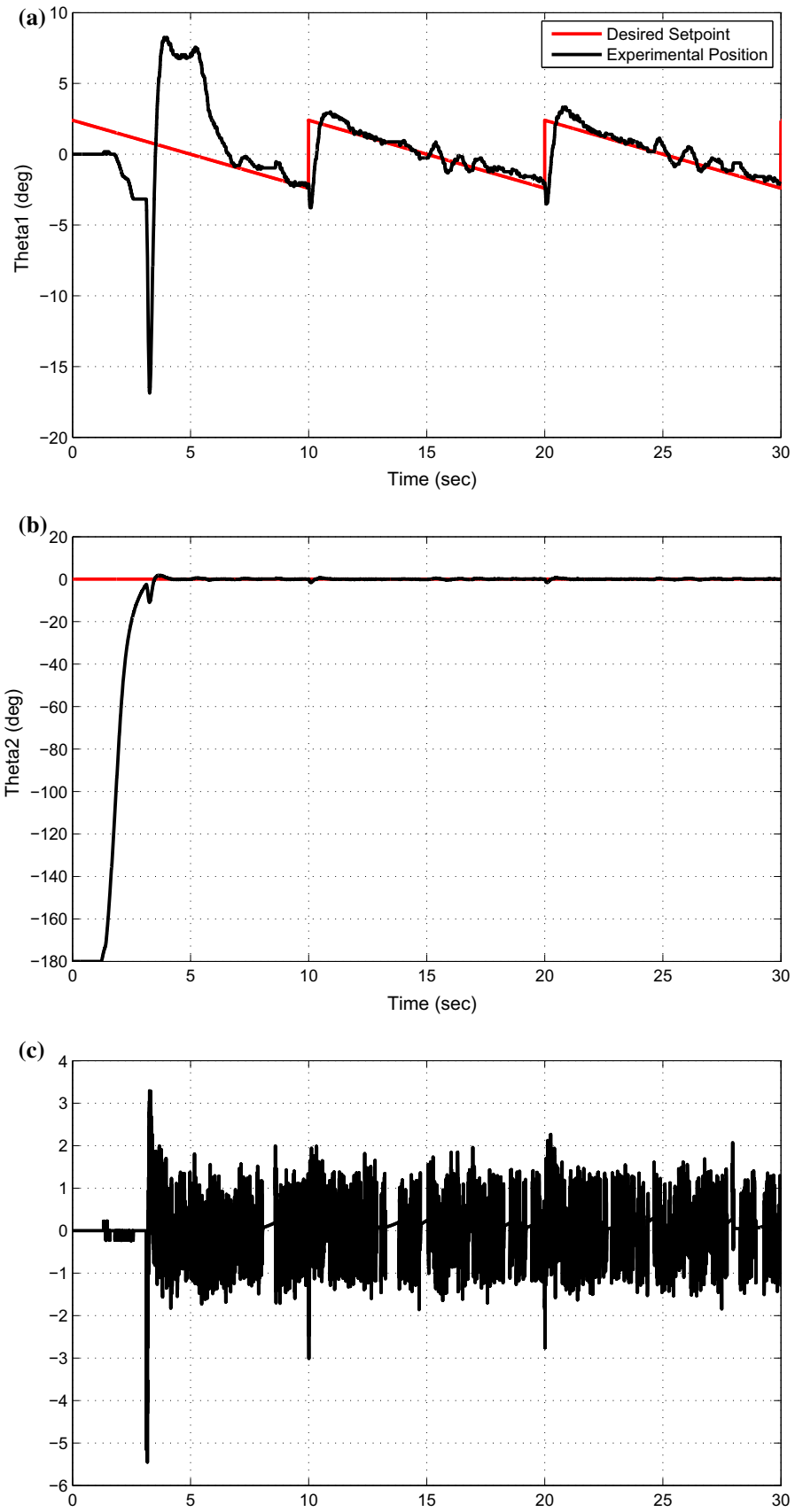

Fig. 12 Experimental results of 2-DOF PID controller with sawtooth wave as reference trajectory **a** rotational position $\theta 1$, **b** pendulum link position $\theta 2$ and **c** control voltage

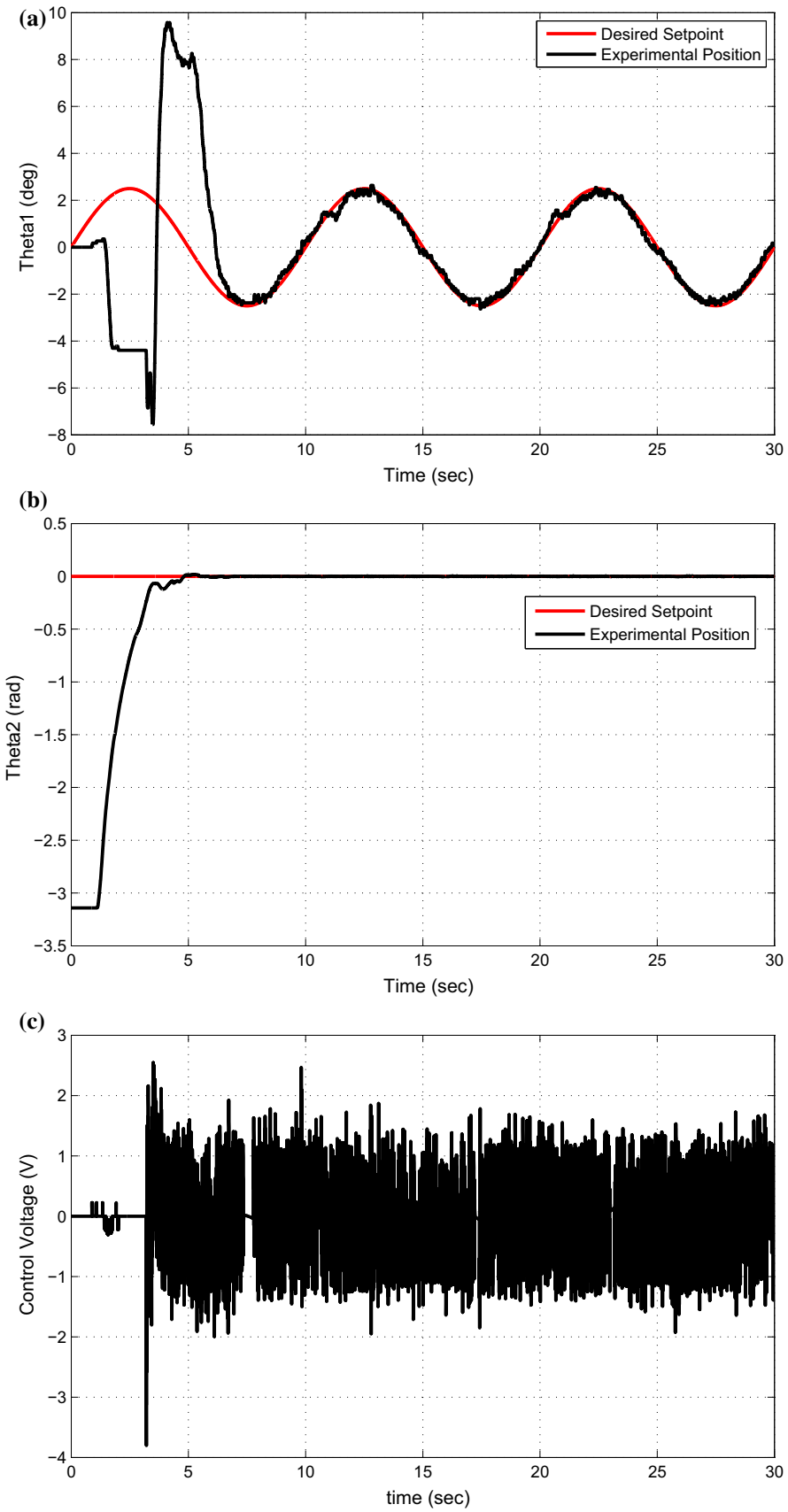

Fig. 13 Experimental results of 2-DOF FOPID controller with sine wave as reference trajectory **a** rotational position $\theta 1$, **b** pendulum link position $\theta 2$ and **c** control voltage

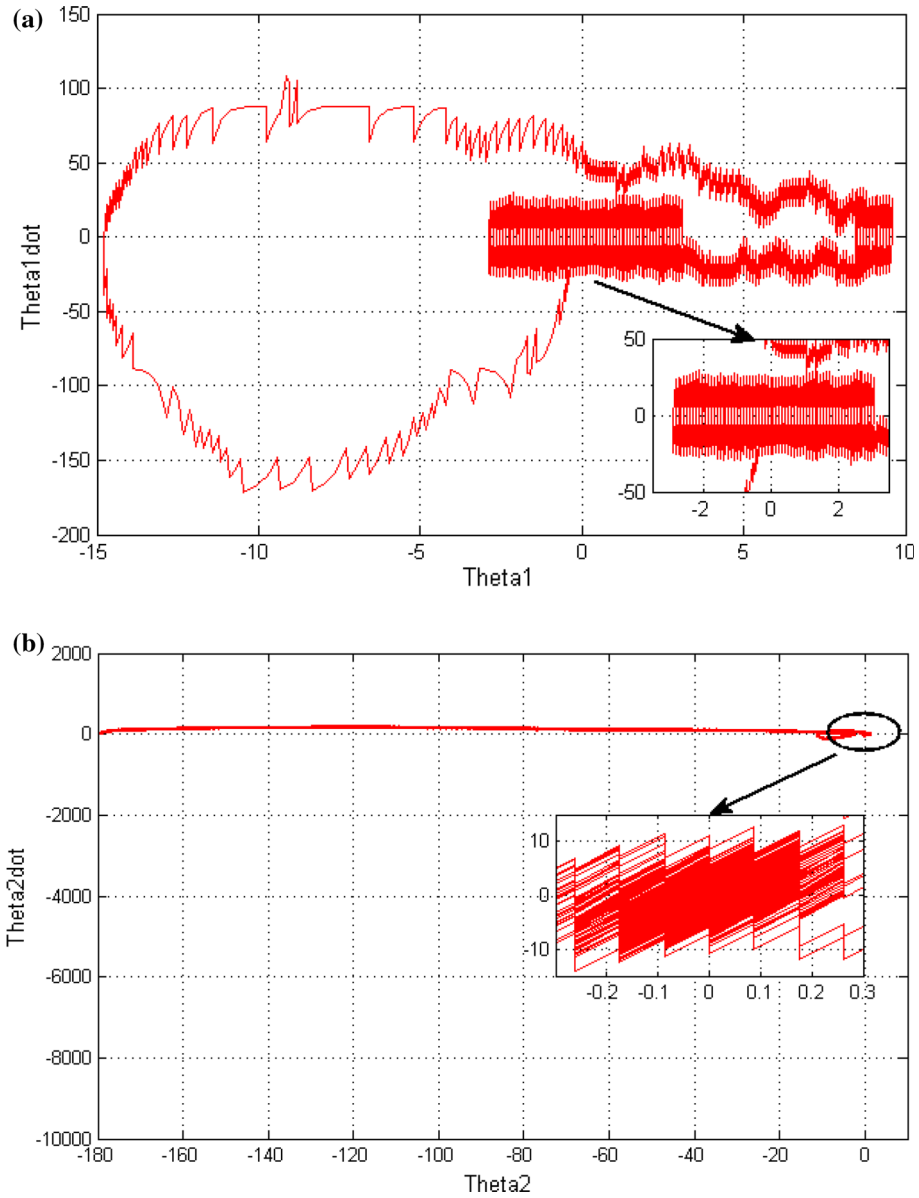

Fig. 14 Phase portrait of 2-DOF FOPID **a** rotational arm and **b** pendulum link

where M_p is defined in (21). The circle is drawn with a radius of d_{min} for determining the robustness of the compensated plant. The plant becomes robust after employing the controller for the external disturbance as seen in Fig. 13. To ensure the robustness, the pendulum was hit manually as an external perturbations at 11, 23.2, 34.2 s, etc. The extensive perturbations are seen at 65 s as shown in Fig. 16a. The pendulum resets within 1.5 s even against the largest amplitude disturbance as shown in Fig. 16b. This establishes the robust nature of the FOPID controller. Corresponding control voltage shows the spikes up to ±6 V at largest external disturbance shown in Fig. 16c.

The robustness is also discussed using experimental phase trajectory shown in Fig. 17. When the pendulum is perturbed externally, the system contains instantaneously more energy to reset the equilibrium point shown in Fig. 17a, b. This more energy shows the large distance between the phase point and the equilibrium point in phase trajectory. After perturbations, trajectory tried to converge at the equilibrium point. However, it contracts into a small confined space rather than a point because stabilizing the pendulum link in upright position system needs continuous energy input. The amount of energy taken by the system depends upon the employed controller.

4.5.2 Stability

Root locus can be used to examine the stability of a given closed-loop system when k is increased from 0 to infinity. Note that for $k = 0$, the open-loop and closed-loop

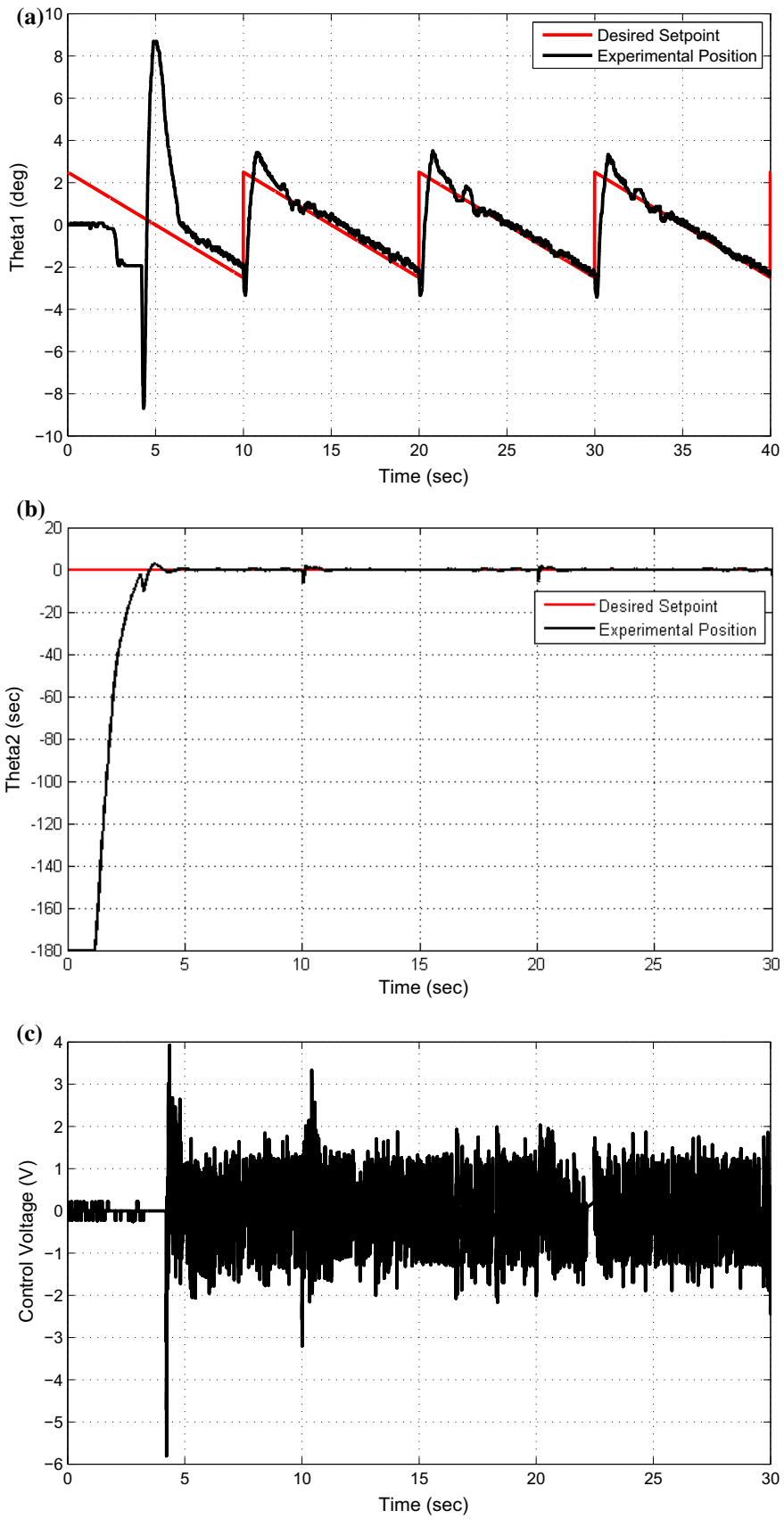

Fig. 15 Experimental results of 2-DOF FOPID controller with sawtooth wave as reference trajectory **a** rotational position $\theta 1$, **b** pendulum link position $\theta 2$ and **c** control voltage

Table 3 Maximum deviation in angular position of RSIP by various controller

Controller	Reference input	Rotational arm (°)	Pendulum link (°)	Control voltage (V)
1-DOF FOPID	Sine waveform	1.4	0.4	±2.35
	Sawtooth waveform	6.3	6	±10
2-DOF PID	Sine waveform	0.66	0.08	±2
	Sawtooth waveform	1.67	1.582	±3.012
2-DOF FOPID	Sine waveform	0.2	0.08	±2
	Sawtooth waveform	1.5	1.2	±2.5

Table 4 Performance indices of error in angular position of rotational arm, pendulum link using 1-DOF FOPID, 2-DOF PID and 2-DOF FOPID controllers

	1-DOF FOPID		2-DOF PID		2-DOF FOPID	
	Rotational arm	Pendulum link	Rotational arm	Pendulum link	Rotational arm	Pendulum link
IAE						
Sine waveform	0.0443	0.07	0.0181	0.047	0.0087	0.0152
Sawtooth waveform	1.8	2.174	0.2807	0.3112	0.1707	0.1903
ISE						
Sine waveform	0.0293	0.0143	0.0093	0.01807	0.0017	0.0074
Sawtooth waveform	0.1345	0.1589	0.1176	0.031	0.00489	0.01

Table 5 Effect of variation in feed-forward parameters on deviation in angular position of rotational arm and pendulum link

Parameter variation	IAE		ISE	
	Rotational arm	Pendulum link	Rotational arm	Pendulum link
Increase in parameters				
$q_1 = 4$	0.012	0.04695	0.0095	0.0217
$q_2 = 3$	0.0088	0.01505	0.0018	0.0074
$q_3 = 0.5$	0.0192	0.047	0.00513	0.0201
$q_4 = 1$	0.00883	0.0157	0.002	0.00793
Decrease in parameters where $q_3 = 0$				
$q_1 = 2$	0.0232	0.048	0.0163	0.0294
$q_2 = 2$	0.009016	0.0152	0.001806	0.0087
$q_4 = 0$	0.00877	0.0154	0.0018	0.0078

poles coincide. Here, open-loop transfer function of the system is pseudo-polynomials with non-integer order instead of integer order. Hence, it is difficult to find stability by simply examining roots. In [24], root locus of commensurate fractional-order open-loop transfer function is plotted in transformed w-plane and again transformed back to the s-plane for analysis purpose. In this, only primary Riemann sheet is analyzed. The issues of root locus branches in secondary Riemann sheets are not addressed. Patil et al. [25] addressed this issue and presented a method of plotting root locus in which all the Riemann sheets are plotted in the same plane (w-plane). Hence, analysis becomes simple and straightforward. Here for determining the stability and robustness, the author is using the same approach.

Fractional-order open-loop transfer function of inverted pendulum system given in Eq. (20) can be represented as in (22),

$$G(s)H(s) = \frac{zfo}{s^{4.7} + 1.87s^{3.7} - 97.61s^{2.7} - 26.69s^{1.7}} \tag{22}$$

where $zfo = s^{4.7} + 275.77s^{3.7} - 219.05s^{3.6} + 1588s^{2.7} - 122.97s^{2.6} + 3059.4s^2 - 428.5s^{1.7} + 9919.1s^{1.6} - 459.31s + 32169s^{0.7} + 37049$.

Transform the above fractional-order transfer function into w-plane by replacing $s^{1/10} = w$. Therefore, integer-order transfer function is given in (23),

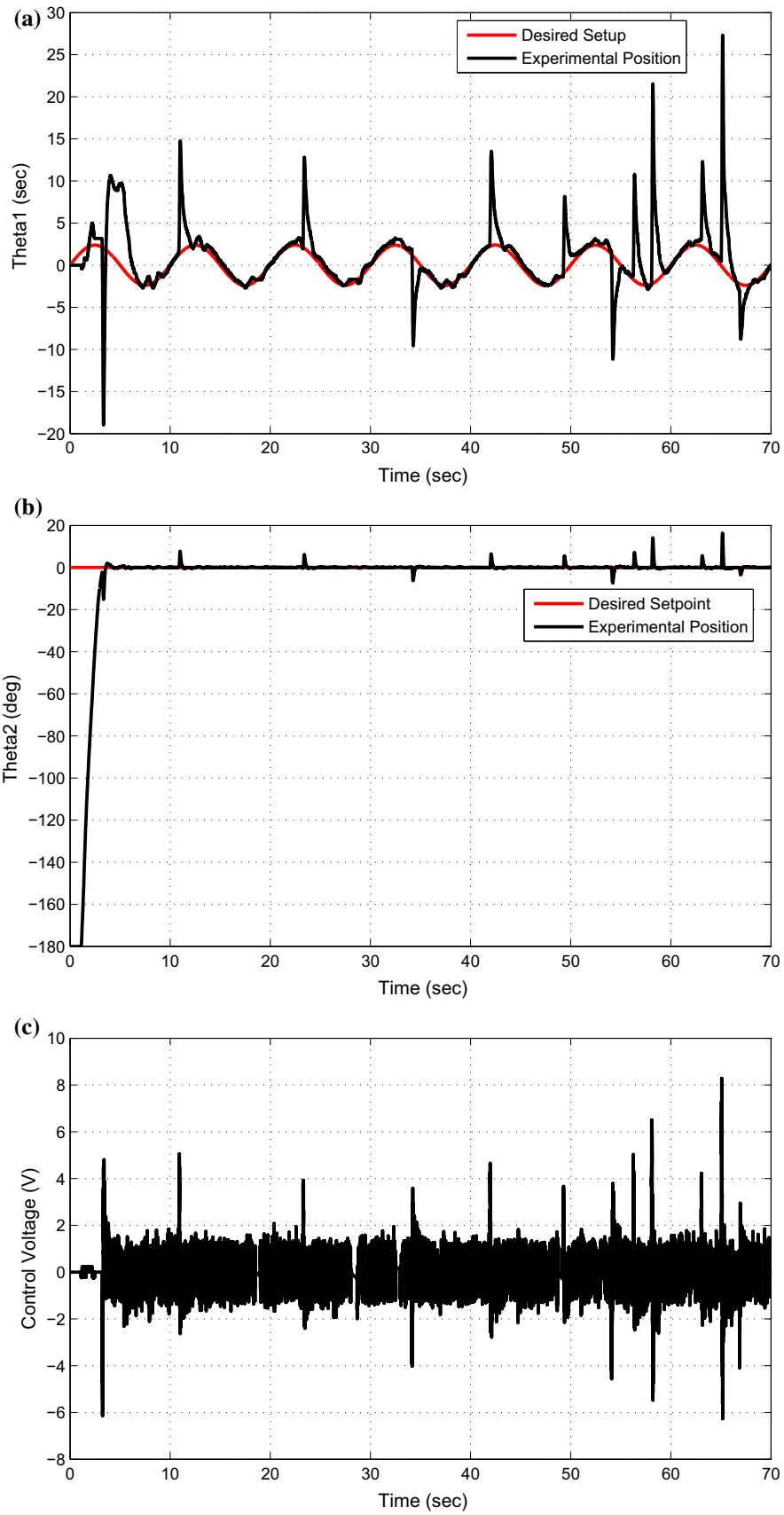

Fig. 16 Experimental response in presence of external perturbation **a** rotational arm position θ_1, **b** pendulum link position θ_2 and **c** control voltage

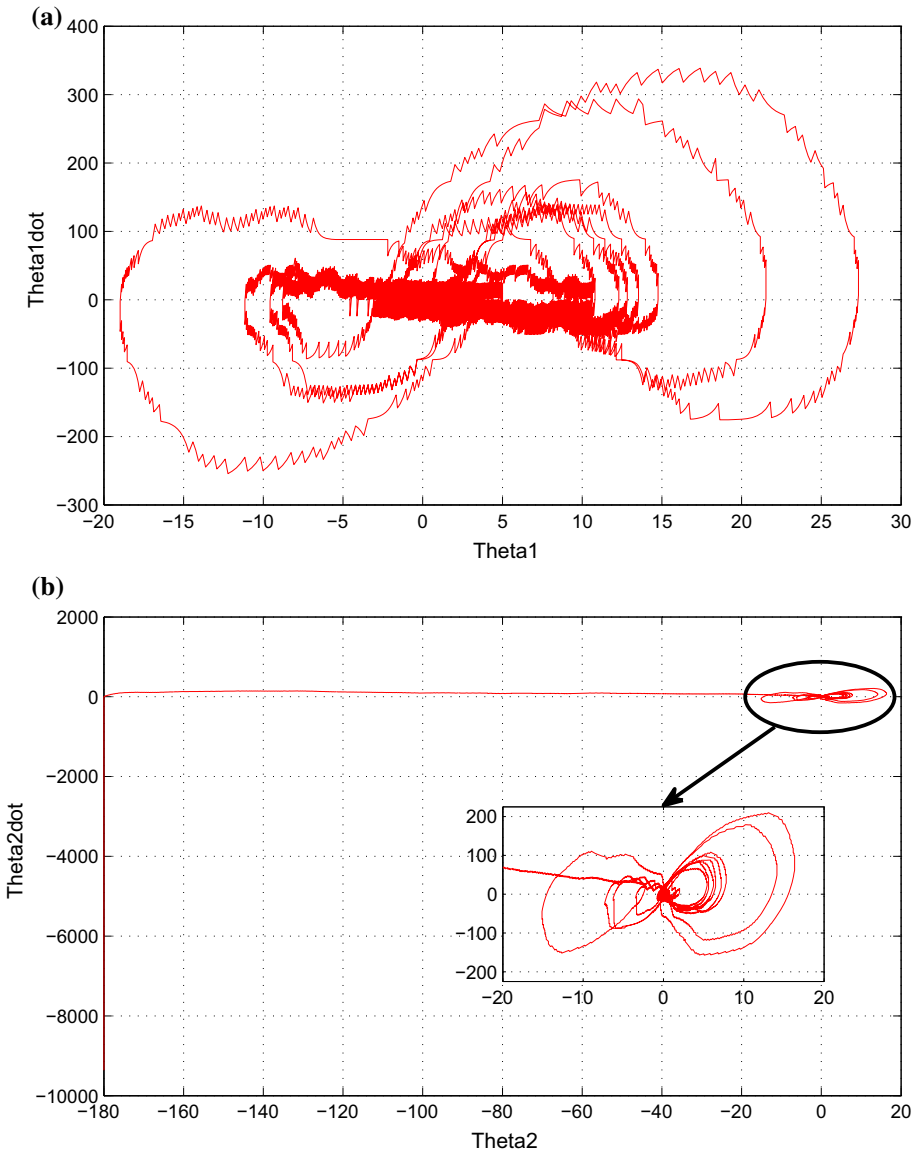

Fig. 17 Experimental phase portrait in the presence of external perturbation **a** rotational arm and **b** pendulum link

$$G(w)H(w) = \frac{zio}{w^{47} + 1.87w^{37} - 97.61w^{37} - 26.69w^{17}} \tag{23}$$

where $zio = w^{47} + 275.77w^{37} - 219.05w^{36} + 1588w^{27} - 122.97w^{26} + 3059.4w^{20} - 428.5w^{17} + 9919.1w^{16} - 459.31w^{10} + 32169w^{7} + 37049$.

The open-loop zeros, poles and their arguments are given in Tables 6 and 7. With this transformation, we have the following observations:

1. The Riemann surface has 10 Riemann sheets shown in Fig, 18a.
2. Principal Riemann sheet (PRS): $-pi/10 < \arg(w) < pi/10$.
3. Unstable region: $-pi/20 < \arg(w) < pi/20$.

The root locus of the system is shown in Fig. 18b. It shows that the system has 4 poles on the principal Riemann sheet. Out of 4 poles, 2 poles are in the unstable region, but at $k = 0.2078$, the root locus branches on primary Riemann sheet moves out of the unstable region. The enlarged view of root locus is shown in Fig. 18c. It shows that all root locus branches are completely outside the unstable region; hence, it is stable for all values of gain $k > 0.2078$. Here it is noteworthy that sufficiently high value of gain is required to moves out the root locus branches from secondary or higher Riemann sheets to primary Riemann sheet (stable or unstable region). Therefore, more no. of poles are in higher no. of Riemann sheet, which means fractional-order PID controller will more robust. This validates the robust nature of controller mentioned in Sect. 4.5.1.

Table 6 Open-loop zeros and the corresponding arguments of system

Open-loop zeros	Arguments in radians	Open-loop zeros	Arguments in radians
$-1.7315 \pm 0.5446j$	2.8363	$-0.6026 \pm 0.8051j$	2.21
$-1.0983 \pm 1.4274j$	2.2262	$-0.0125 \pm 1.24j$	1.5805
$-0.0755 \pm 1.7692j$	1.6131	$-0.1881 \pm 1.0872j$	1.7417
$0.9405 \pm 1.4415j$	0.9925	$1.2543 \pm 0.2612j$	0.2052
$1.5522 \pm 0.5611j$	0.3468	$1.1034 \pm 0.2591j$	0.2305
$-1.1674 \pm 0.3969j$	2.81	$1.0933 \pm 0.4778j$	0.4119
-1.0971	3.14	$0.7660 \pm 0.9856j$	0.9099
$-1.0575 \pm 0.1219j$	3.0262	$0.8697 \pm 0.8288j$	0.7162
$-0.9836 \pm 0.5693j$	2.6164	$0.8879 \pm 0.4860j$	0.5007
$0.8364 \pm 0.7374j$	2.2773	$0.2726 \pm 1.1629j$	1.3402
$0.7007 \pm 0.9646j$	2.1986	$0.5288 \pm 0.9836j$	1.077
$0.4730 \pm 1.0866j$	1.9810	$0.2070 \pm 0.9631j$	1.3588

Table 7 Open-loop poles and the corresponding arguments of system

Open-loop poles	Arguments in radians	Open-loop poles	Arguments in radians
0 (19 Repetative poles)	0	$-1.2087 \pm 0.3927j$	2.8260
-1.2432	3.14	$-1.0058 \pm 0.7307j$	2.5120
$-0.7470 \pm 1.0282j$	2.199	$-0.3842 \pm 1.182j$	1.8849
$\pm 1.2709j$	1.570	$0.3842 \pm 1.1823j$	1.2566
$0.7470 \pm 1.0282j$	0.9429	1.2432	0
$1.2087 \pm 0.3927j$	0.3141	$1.0058 \pm 0.7307j$	0.62828
-0.8884	3.14	$-0.7187 \pm 0.5222j$	2.5132
$-0.2745 \pm 0.8449j$	1.8849	$0.2745 \pm 0.8449j$	1.2566
0.884	0	$0.7187 \pm 0.5222j$	0.6283

5 Conclusion and Future Work

Various techniques with traditional PID controller have been found in the literature to control the RSIP system. Generally speaking, these techniques provide good results; nonetheless, improvement is aught in the smooth tracking (negligible oscillations) and reducing the peaks at sudden changes in reference trajectory. The 2-DOF FOPID controller helps to mitigate the said difficulties. The advantages of this control scheme are stated:

- 2-DOF controller magnified the robustness of the system toward perturbations and trajectory tracking, whereas the incorporation of fractional-order operators has increased the flexibility in selection of controller parameters.
- The sustained oscillations in steady-state response of angular displacement in rotational arm have been reduced up to 76%.
- The required average control voltage has been reduced.
- The intensity of spikes has lessened during a sudden change in the reference trajectory.
- Total 10 Riemann sheets were found in Riemann surface, and out of 47 poles, only 4 poles were found in the principle Riemann sheet. All poles have moved out of the stable region for any value of $k > 0.2078$, which shows the more stable and robust nature of the controller.
- The values of IAE and ISE have been found smaller for the angular deviation in the rotational arm and pendulum link for 2-DOF FOPID controller as compared to 2-DOF PID and 1-DOF FOPID controllers.

This study analyzes and synthesizes a fractional-order-based 2-DOF controller for a nonlinear RSIP system. Based on the literature survey, some related issues for future research works are outlined as follows:

- It is noteworthy that no fractional-order modeling or fractional identification of RSIP system has been found in the literature. Therefore, fractional identification should be further carried out.
- The results in the study were obtained mainly for balancing the pendulum link, and here, the pendulum was swung up manually. However, nonlinear control techniques such as fractional sliding mode, T–S-based fuzzy logic control, piecewise H_∞ control, Lyapunov function-based nonlinear control and predictive control, etc. [26–31] can further

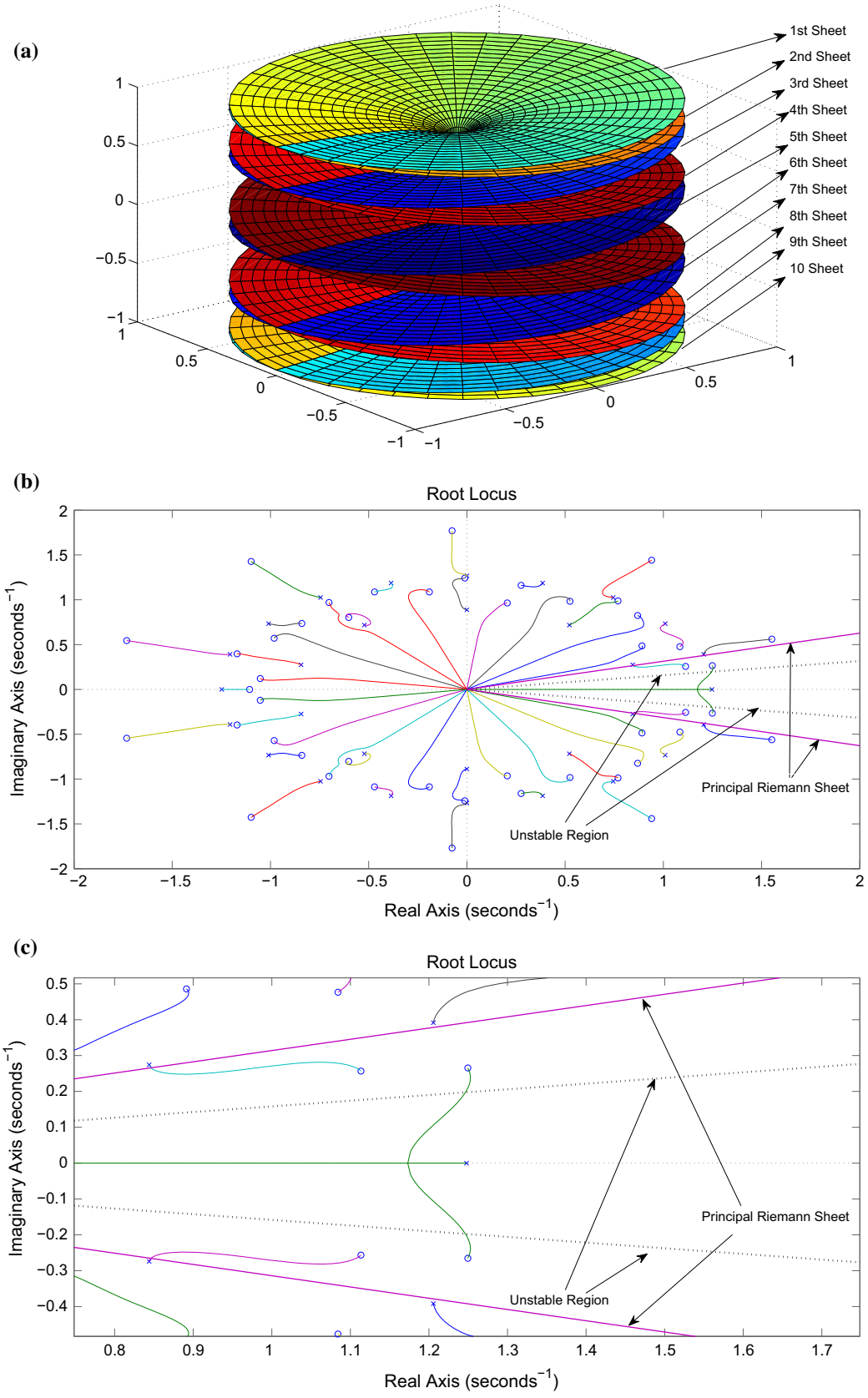

Fig. 18 Root locus of inverted pendulum with fractional-order controller **a** Riemann surface for $w = s^{1/10}$, **b** root locus of transformed w-plane and **c** close view of root locus of transformed w-plane

be tried to swing up the pendulum. The insights from these experiments will also provide some guidelines for practical applications of the proposed approaches.

– In the present study, linearized control scheme has been used to design a controller. However, some typical nonlinear control schemes such as fuzzy logic model-based nonlinear networked control strategy, networked industrial processes based on optimal control, networked multiple mobile robots, etc., might be further used to design a fractional controller [32,33]. In this way, strengths and weaknesses of the proposed methods would be critically assessed.
– Further, a standalone unit of a digital fractional controller using any nonlinear control methods such as sliding mode topology based on microprocessor or FPGA can be designed for RSIP system.

By taking the cognizance of the advantages of these experiments, the proposed fractional scheme will also provide some guidelines for practical applications such as robotic arms, mobile wheeled inverted pendulum (Segway) and humanoid robots.

References

1. Ghosh, A.; Krishnan, T.R.; Subudhi, B.: Robust proportional–integral–derivative compensation of an inverted cart-pendulum system: an experimental study. IET Control Theory Appl. **6**(8), 1145–1152 (2012)
2. Zilic, T.; Pavkovic, D.; Zorc, D.: Modeling and control of a pneumatically actuated inverted pendulum. ISA Trans. **48**, 327–335 (2009)
3. Casanova, V.; Alcaina, J.; Salt, J.; Piza, R.; Cuenca, A.: Control of the rotary inverted pendulum through threshold-based communication. ISA Trans. **62**, 357–366 (2016)
4. Magin, R.; Ortigueira, M.D.; Podlubny, I.; Trujillo, J.: Review on the fractional signals and systems. Signal Process. **91**, 350–371 (2011)
5. Francisco, G.A.J.; Juan, R.G.; Roberto, R.H.J.; Manuel, G.C.: Fractional RC and LC electrical circuits. Ing. Investig. Tecnol. **15**(2), 311–319 (2014)
6. Grzesikiewicz, W.; Wakulicz, A.; Zbiciak, A.: Non-linear problems of fractional calculus in modeling of mechanical systems. Int. J. Mech. Sci. **70**, 90–98 (2013)
7. Pan, I.; Das, S.: Fractional order fuzzy control of hybrid power system with renewable generation using chaotic PSO. ISA Trans. **62**, 19–29 (2016)
8. Podlubny, I.: Fractional order systems and $PI^{\lambda}D^{\mu}$ controllers. IEEE Trans. Autom. Control **44**(1), 208–214 (1999)
9. Martin, F.; Monje, C.A.; Moreno, L.; Balaguer, C.: DE-based tuning of $PI^{\lambda}D^{\mu}$ controllers. ISA Trans. **59**, 398–407 (2015)
10. Keyser, R.D.; Muresan, C.I.; Ionescu, C.M.: A novel auto-tuning method for fractional order PI/PD controllers. ISA Trans. **62**, 268–275 (2016)
11. Das, S.; Pan, I.; Das, S.; Gupta, A.: Improved model reduction and tuning of fractional-order $PI^{\lambda}D^{\mu}$ controllers for analytical rule extraction with genetic programming. ISA Trans. **51**, 237–261 (2012)
12. Ghosh, A.; Krishnan, T.R.; Tejaswy, P.; Mandal, A.; Pradhan, J.K.; Ranasingh, S.: Design and implementation of a 2-DOF PID compensation for magnetic levitation systems. ISA Trans. **53**, 1216–1222 (2014)
13. Li, M.; Zhou, P.; Zhao, Z.; Zhang, J.: Two-degree-of-freedom fractional order-PID controllers design for fractional order processes with dead-time. ISA Trans. **61**, 147–154 (2016)
14. Sharma, R.; Gaur, P.; Mittal, A.P.: Performance analysis of two-degree of freedom fractional order PID controllers for robotic manipulator with payload. ISA Trans. **58**, 279–291 (2015)
15. Vilanova, R.; Alfaro, V.M.; Arrieta, O.: Simple robust autotuning rules for 2-DoF PI controllers. ISA Trans. **51**, 30–41 (2012)
16. User manual inverted pendulum experiment, Quanser (2012)
17. Charef, A.: Analogue realisation of fractional order integrator, differentiator and fractional $PI^{\lambda}D^{\mu}$ controller. IEE Proc. Control Theory Appl. **153**(6), 714–720 (2006)
18. Oustaloup, A.; Levron, F.; Mathieu, B.; Nanot, F.M.: Frequency band complex noninteger differentiator: characterization and synthesis. IEEE Trans. Circuits Syst. I Fundam. Theory Appl. **47**(1), 25–39 (2000)
19. Djouambi, A.; Charef, A.; Besancon, A.V.: Optimal approximation, simulation and analog realization of the fundamental fractional order transfer function. Int. J. Appl. Math. Comput. Sci. **17**(4), 455–462 (2007)
20. Meng, L.; Xue, D.: A new approximation algorithm of fractional order system models based optimization. J. Dyn. Syst. Meas. Control **134**, 1–7 (2012)
21. Xue, D.; Zhao, C.; Chen, Y.Q.: A modified approximation method of fractional order system. In: Proceedings of the 2006 IEEE International Conference on Mechatronics and Automation, Luoyang, China (2006)
22. Teplijakov, A.; Petlenkov, E.; Belikov, J.: FOMCON: a MATLAB toolbox for fractional-order system identification and control. Int. J. Microelectron. Comput. Sci. **2**(2), 51–62 (2011)
23. Wolovich, W.A.: Automatic Control Systems. Oxford University Press, Oxford (1993)
24. De, A.; Sen, S.: Root locus method for any fractional order commensurate system. In: Proceedings of the 2011 IEEE Students' Technology Symposium, IIT Kharagpur, India, pp. 323–328 (2011)
25. Patil, M.D.; Vyawahare, V.A.; Bhole, M.K.: A new and simple method to construct root locus of general fractional-order systems. ISA Trans. **53**, 380–390 (2014)
26. Qiu, J.; Tian, H.; Lu, Q.; Gao, H.: Nonsynchronized robust filtering design for continuous-time TS fuzzy affine dynamic systems based on piecewise Lyapunov functions. IEEE Trans. Cybern. **43**(6), 1755–1766 (2013)
27. Qiu, J.; Ding, S.X.; Gao, H.; Yin, S.: Fuzzy-model-based reliable static output feedback $H-\infty$ control of nonlinear hyperbolic PDE systems. IEEE Trans. Fuzzy Syst. **24**(2), 388–400 (2016)
28. Qiu, J.; Wei, Y.L; Wu, LG.: A novel approach to reliable control of piecewise affine systems with actuator faults. IEEE Trans. Circuits Syst II: Express Briefs. (2016). doi:10.1109/TCSII.2016.2629663
29. Gawthrop, P.J.; Wang, L.: Intermittent predictive control of an inverted pendulum. Control Eng. Pract. **14**, 1347–1356 (2006)
30. Mills, A.; Wills, A.; Ninness, B.: Nonlinear model predictive control of an inverted pendulum. In: Proceedings of the American Control Conference, St. Louis, pp. 2335–2340 (2009)
31. Mujumdar, A.; Tamhane, B.; Kurode, S.: Fractional order modeling and control of a flexible manipulator using sliding modes. In: American Control Conference (ACC), Portland, Oregon, USA, pp. 2011–2016 (2014)
32. Qiu, J.; Wang, T.; Yin, S.; Gao, H.: Data-based optimal control for networked double-layer industrial processes. IEEE Trans. Ind. Electron. **64**, 4179–4186 (2017)
33. Qiu, J.; Gao, H.; Ding, S.X.: Recent advances on fuzzy-model-based nonlinear networked control systems: a survey. IEEE Trans. Ind. Electron. **63**(2), 1207–1217 (2016)